Low-Dimensional Reduced-Order Models for Statistical Response and Uncertainty Quantification: Barotropic Turbulence with Topography

Di Qi[a,*], Andrew J. Majda[a]

[a]*Department of Mathematics and Center for Atmosphere and Ocean Science, Courant Institute of Mathematical Sciences, New York University, New York, NY 10012*

Abstract

A low-dimensional reduced-order statistical closure model is developed for quantifying the uncertainty to changes in forcing in a barotropic turbulent system with topography involving interactions between small-scale motions and a large-scale mean flow. Imperfect model sensitivity is improved through a recent mathematical strategy for calibrating model errors in a training phase, where information theory and linear statistical response theory are combined in a systematic fashion to achieve the optimal model parameters. Statistical theories about a Gaussian invariant measure and the exact statistical energy equations are also developed for the truncated barotropic equations that can be used to improve the imperfect model prediction skill. A stringent paradigm model of 57 degrees of freedom is used to display the feasibility of the reduced-order methods. This simple model creates large-scale zonal mean flow shifting directions from westward to eastward jets with an abrupt change in amplitude when perturbations are applied, and prototype blocked and unblocked patterns can be generated in this simple model similar to the real natural system. Principal statistical responses in mean and variance can be captured by the reduced-order models with desirable accuracy and efficiency with only 3 resolved modes. An even more challenging regime with non-Gaussian equilibrium statistics using the fluctuation equations is also tested in the reduced-order models with accurate prediction using the first 5 resolved modes. These reduced-order models also show potential for UQ and prediction in more complex realistic geophysical turbulent dynamical systems.

Keywords: Reduced-order methods, topographic barotropic system, statistical responses, uncertainty quantification

1. Introduction

Turbulent dynamical systems characterized by a large dimensional phase space and many degrees of strong instabilities transferring energy throughout the system are ubiquitous in science and engineering [1, 2, 3, 4]. Situations of obvious importance in atmosphere and ocean science occur when smaller-scale motions have a significant feedback and interaction with a larger-scale mean flow [5, 6, 7]. The feedbacks and interaction induce instability that can make the system very sensitive to even small changes in external forcing perturbations. One prototype situation of this sort occurs in the interaction of large-scale and small-scale components of barotropic flow over topography via topographic stress. The influence of large-scale anisotropic topographic variations on the fluid forms alternative blocked and unblocked states relative to the model sensitivity to the forcing. The simplest set of equations that meaningfully describes the motion of the large-scale geophysical flows is given by the quasi-geostrophic barotropic equations [3, 4]. They are the result of "filtering out" the fast gravity waves from the rotating barotropic equations. The multiple equilibrium states of this barotropic system with dissipation and single-mode topography are studied in [8, 9], suggesting the possible importance as model states of atmospheric blocking and changes due to variations in external forcing. The system can also be extended to a number of important climate models directly such as two-layer models or barotropic flow on the sphere, characterizing a wider category of realistic phenomena from nature.

*Corresponding author
Email addresses: qidi@cims.nyu.edu (Di Qi), jonjon@cims.nyu.edu (Andrew J. Majda)

The turbulent nature of the dynamical systems characterized by a large number of positive Lyapunov exponents with instability requires a probabilistic description for the dynamical evolution of the system. Statistical uncertainty quantification (UQ) concerns about capturing responses to the change in forcing in such turbulent systems using imperfect models due to both the lack of physical understanding and the overwhelming computational demands of Monte-Carlo simulation in a large dimensional phase space [10, 4, 11]. Most earlier works in statistical turbulence involve assumptions of homogeneity and isotropy without a mean flow or approximate the nonlinear terms in the equations for the mean flow and fluctuating interactions by linear stochastic models [12, 13, 14, 1]. One central issue in contemporary climate science requires a systematic methodology that can recover the crucial statistical features of the turbulent systems in statistical equilibrium (model fidelity) and improve the imperfect model prediction skill in response to anisotropic perturbations like the climate change (model sensitivity) at the same time [15, 11, 16] for a wide variety of forcing scenarios.

Fluctuation dissipation theorem (FDT) for complex systems offers a way to predict linear first-order statistical responses utilizing the linear response theory [17, 18, 19, 20] requiring only measurements in the unperturbed system. Despite some success in complex systems, this method is hampered by the fundamental limitation to parameter regimes with linear statistical response. Thus new strategies for imperfect low-order models on subspace are important and a main theme of present research [21, 22, 11]. In [23] a new energy principle with the exact treatment of the nonlinear inhomogeneous statistical energy exchange between the mean and fluctuations are proposed, which are amenable to systematic low-order closure methods for prediction and uncertainty quantification with high skill [11].

In this paper, we consider the development of reduced-order models that have the ability to capture the statistical sensitivity in the principal directions of the system, while at the same time reducing the high computational costs that usually form the inherent obstacle for resolving the geostrophic turbulence. The basic idea of the statistical reduced-order methods are introduced in [11] and the feasibility has been tested successfully on a 40-dimensional Lorenz-96 system in various dynamical regimes. The expensive nonlinear interactions in the turbulent system are replaced by nonlinear *statistical energy* dependent damping and noise corrections, which are calibrated carefully according to the true equilibrium higher-order statistics in a training phase before the prediction. Imperfect model errors introduced through this model approximation are improved through a systematic framework measuring the kicked *linear response operator* under the *relative entropy* metric with only unperturbed equilibrium information used [15, 16]. In order to apply this idea to the much more complicated topographic barotropic system interacting with mean flow, statistical theories are developed following a general framework for the one-layer barotropic flow as well as for the fluctuation equations concentrating on the deviations about the mean state. With a carefully designed damping and random noise forcing terms applied on the set of equations, a Gaussian invariant measure can be reached in the unperturbed statistical steady state. The linear response operator thus can be derived in explicit forms, offering a convenient way to measure the imperfect model errors in the training phase efficiently. Finally, the specific dynamical equations for statistical energy according to the conserved quantities (that is, energy, enstrophy, and the pseudo-energy in fluctuation equations) are developed following the general formulation in [23], offering a desirable scaling operator that can further improve the model sensitivity in the imperfect quantification.

In testing the validity of the reduced-order schemes in the topographic barotropic system interacting with a mean flow, a stringent paradigm model [24, 25] of 57 degrees of freedom with a large scale zonal (east-west) jet and interacting topographic Rossby waves is proposed as the perfect system. Prototype topographic blocking and unblocking patterns are produced in this model, with topographic stress as the only transfer mechanism between small and large scales. These patterns bear some qualitative resemblance to those observed in recent laboratory experiments on topographic blocking [26, 27]. Another important feature that can be observed in this simple system is the change of direction in the mean zonal jet. As the external deterministic forcing perturbation increases gradually, the zonal mean flow shifts from a west-going jet to eastward with an abrupt change of amplitude implying a bifurcation in the flow statistics. Below it is shown that using a reduced-order model in only 3-dimensional resolved subspace, the principal statistics in first and second moments including the shifting jet directions can be captured with desirable accuracy and efficiency. A further stringent test case is developed for the fluctuation equations with non-zero deterministic forcing in the unperturbed climate, where a non-Gaussian equilibrium measure is generated like many realistic situations. Despite the unavoidable model errors from higher-order statistics in this tougher case, the low-order closure approximation models with 5 resolved modes display uniform ability in predicting responses to various external perturbations through the proposed information-response framework.

The remainder of the paper is arranged in the following way. Section 2 introduces the basic topographic barotropic

equations of interest in this paper, and the related fluctuation equations about the presumed mean state are also described. Important conserved quantities in the systems are shown for later use. Then statistical theories about the barotropic flow are developed in Section 3. A general theory for an abstract system with quadratic energy-conserving nonlinearity of systems is described in the first place. Developments of statistical theories about the barotropic system follow next according to the the general theoretical framework. A useful Gaussian invariant measure together with the exact formulation of linear response operators as well as the detailed statistical energy equations is derived under the barotropic framework. Imperfect models with statistical closure strategies and systematic calibration that guarantees statistical equilibrium fidelity and optimal model sensitivity are then discussed in Section 4. A general strategy for the reduced-order model algorithm is summarized in the end of this section. The performances of the reduced-order closure models in response to different kinds of perturbations in different regimes are displayed in both the barotropic equations and the fluctuation equations in Section 5. Conclusions and future work are summarized in Section 6.

2. Basic equations and conserved quantities

First we describe the systems of interest in this paper, that is, the two-dimensional barotropic flow including instability from topographic stress and zonal mean flow interaction. The barotropic flow can be viewed as a vertically averaged one-layer system which generates many interesting and representative features found in the real atmosphere and ocean. Especially, the fluctuation part about the mean state in the flow is always of special interest in many situations and is worth being considered individually in the dynamics. Both the original topographic barotropic flow and the related fluctuation equations display representative dynamical features with relatively simple structure in the equations as a desirable paradigm for testing models for geophysical turbulence. In investigating the statistical structures of the turbulent system, conserved quantities play a decisive role both in theoretical analysis and the development of numerical methods [12, 4]. Therefore the crucial conserved quantities in this barotropic flow are also reviewed here and will be used in the following parts of the paper in helping to develop reduced-order schemes.

2.1. Topographic barotropic system with a zonal mean flow

A basic group of simple models that incorporate the essential structures in geostrophic turbulence is the ideal barotropic quasi-geostrophic equations on a two-dimensional $2\pi \times 2\pi$ periodic geometry with a large-scale zonal mean flow and topographic effect [28, 27, 4, 5]. In general, the topographic barotropic flow on a rotational β-plane with dissipation and forcing can be formulated as

$$\frac{\partial \omega}{\partial t} + \nabla^{\perp}\psi \cdot \nabla q + \beta \frac{\partial \psi}{\partial x} + U\frac{\partial q}{\partial x} = -\mathcal{D}(\Delta)\psi + \mathcal{F}(\mathbf{x}, t) + \Sigma(\mathbf{x})\dot{W}(t), \tag{2.1a}$$

$$\frac{dU}{dt} + \oint \frac{\partial h}{\partial x}\psi(t) = -\mathcal{D}_0 U + \mathcal{F}_0(t) + \Sigma_0 \dot{W}_0(t), \tag{2.1b}$$

where $q = \omega + h$, $\omega = \Delta\psi$ are the potential vorticity and relative vorticity respectively; and ψ is the stream function; h is the topographic structure while q is advected by the velocity field of the flow, $\mathbf{v} = \nabla^{\perp}\psi \equiv \left(-\partial_y\psi, \partial_x\psi\right)$. Throughout the rest of this paper, we use the spatial-averaged integration

$$\oint f \equiv \frac{1}{4\pi^2}\int_{-\pi}^{\pi}\int_{-\pi}^{\pi} f(x, y)\, dxdy,$$

defined in the periodic domain $[-\pi, \pi] \times [-\pi, \pi]$. The large-scale mean flow U is coupled with small-scale vortical modes through the topographic stress; this effect is the direct analogue for periodic geometry of the change in time of angular momentum due to mountain torque in spherical geometry [4, 29]. The equations (2.1a) and (2.1b) provide a closed system describing the anisotropic interaction between large and small scales through the geophysical effects from U, β, and the topography, h; and maintaining the important quadratic invariants of the flow. The evolution of U in (2.1b) enforces the conservation of energy and enstrophy without damping and forcing terms on the right had sides of the equations. High-order nonlinear energy and enstrophy conserving interactions between modes in (2.1) make the true statistical structure of the system quite complicated.

On the right hand sides of the equations, we assume fairly general *dissipation and forcing operators* for both small and large scale variables. In small scale, the general dissipation operator may encompass radiative damping ($l = 0$), Ekman drag dissipation ($l = 1$), Newtonian (eddy) viscosity ($l = 2$), and hyper-viscosity ($l \geq 3$) in the form as

$$\mathcal{D}(\Delta) = \sum_{l=0}^{L} d_l (-\Delta)^l, \quad d_l \geq 0. \tag{2.2}$$

The constant damping $-\mathcal{D}_0 U$ in the large-scale mean flow represents momentum damping. The forcing operator is decomposed into a deterministic component (e.g. radiative heating, surface wind stress, etc.), and a random component (e.g. convective storms, unresolved baroclinic instability processes on small length scales, random wind stress, etc.) represented by Gaussian white noises. The deterministic forcing component can be defined through the spectral expansion

$$\mathcal{F}(\mathbf{x}, t) = \sum \hat{\mathcal{F}}_{\mathbf{k}}(t) e^{i\mathbf{k}\cdot\mathbf{x}} + c.c. \tag{2.3}$$

where $c.c.$ represents the complex conjugate so that the forcing term will always take real values. The random Gaussian noise forcing is essential for generating a Gaussian invariant measure in the unperturbed equilibrium (though small amplitude (Σ_0, Σ) in the random forcing term is sufficient).

Two conserved quantities, which will play a decisive role in the statistical theory and development about reduced-order methods, can be found in the barotropic flow (2.1). They are the *total kinetic energy, E*, and the *large-scale enstrophy,* $\mathscr{E}$, defined as

$$\begin{aligned} E &= \frac{1}{2}U^2 + \frac{1}{2}\oint |\nabla\psi|^2, \\ \mathscr{E} &= \beta U + \frac{1}{2}\oint (\omega + h)^2. \end{aligned} \tag{2.4}$$

In the absence of dissipation and forcing on the right hand sides of (2.1), the two quantities in (2.4) will always stay conserved as the flow evolves in time. This is due to the energy and enstrophy conservation of the nonlinear interactions as well as the skew-symmetry of the linear operators from the rotation and mean flow effects. Detailed discussion about all these conservation quantities can be found in Chapter 1 of [4] and [23].

2.2. Fluctuation equations of the one-layer topographic barotropic flow

In many problems in geophysical fluids, the time-averaged unperturbed mean state (i.e. the climate) is assumed to be known with reasonable accuracy, then the statistical fluctuations about the unperturbed mean state become the quantities of special interest [28, 4, 24]. We decompose the state variables in the original barotropic system (2.1) into the time-averaged unperturbed equilibrium mean, $\left(\bar{U}_{\text{eq}}, \bar{\psi}_{\text{eq}}\right)$, and the fluctuations about the mean states, $\left(\tilde{U}, \tilde{\psi}\right)$, thus the original state variables have the decomposition

$$U(t) = \bar{U}_{\text{eq}} + \tilde{U}(t), \ \psi(\mathbf{x}, t) = \bar{\psi}_{\text{eq}}(\mathbf{x}) + \tilde{\psi}(\mathbf{x}, t). \tag{2.5}$$

A special form of the exact mean steady state with linear dependence between the stream function and potential vorticity is often assumed as [4]

$$\bar{q}_{\text{eq}} = \Delta\bar{\psi}_{\text{eq}} + h = \mu\bar{\psi}_{\text{eq}}, \quad \bar{U}_{\text{eq}} = -\beta/\mu. \tag{2.6}$$

By subtracting the time-averaged mean states (2.6) from the original equations (2.1), the **fluctuation equations of the barotropic flow** become

$$\begin{aligned} &\frac{\partial\tilde{\omega}}{\partial t} + \nabla^{\perp}\tilde{\psi}\cdot\nabla\tilde{\omega} + \nabla^{\perp}\bar{\psi}_{\text{eq}}\cdot\nabla\left(\tilde{\omega} - \mu\tilde{\psi}\right) \\ &\quad + \tilde{U}\frac{\partial}{\partial x}\left(\tilde{\omega} + \bar{q}_{\text{eq}}\right) + \bar{U}_{\text{eq}}\frac{\partial}{\partial x}\left(\tilde{\omega} - \mu\tilde{\psi}\right) = -\mathcal{D}(\Delta)\tilde{\psi} + \mathcal{F}(\mathbf{x}, t) + \Sigma(\mathbf{x})\dot{W}(t), \end{aligned} \tag{2.7a}$$

$$\frac{d\tilde{U}}{dt} + \oint \frac{\partial h}{\partial x}\tilde{\psi}(t) = -\mathcal{D}_0\tilde{U} + \mathcal{F}_0(t) + \Sigma_0\dot{W}_0(t). \tag{2.7b}$$

with $\tilde{\omega} = \Delta\tilde{\psi}$, the fluctuation components of the vorticity and stream function respectively. In the small-scale vorticity dynamics (2.7a), the first row is due to the advection terms, while the second row is from the β-effect and interaction

with the fluctuating mean flow. Similar damping and forcing terms are added in both small and large scales on the right hand sides of (2.7). In the rest parts of the paper, for a neater representation, we abuse the notation a little and neglect the 'tildes' on the fluctuation components.

In this fluctuation equation (2.7), neither the energy nor the enstrophy in the fluctuation part keeps conserved as the quantities in (2.4) due to the inclusion of mean state $\left(\bar{U}_{\rm eq}, \bar{\psi}_{\rm eq}\right)$ in (2.7a). Still one important conserved quantity can be constructed as the *pseudo-energy* $\tilde{E}$ through a linear combination of the energy and enstrophy in the fluctuation part

$$\tilde{E} = \mathscr{E} + \mu E = \frac{1}{2}\tilde{U}^2 + \frac{1}{2}\oint \tilde{\omega}\left(\tilde{\omega} - \mu\tilde{\psi}\right). \tag{2.8}$$

The pseudo-energy in (2.8) is often more useful since it combines the two important conserved quantities, E and $\mathscr{E}$. The conservation of statistical theory can predict equipartition of energy under this pseudo-energy coordinate and imply the nonlinear stability of the climate mean state [4]. In the next section, it can be seen that the Gibbs measure for fluctuations can be derived from this pseudo-energy, and this leads to prediction of a Gaussian invariant measure about the statistical mean state in the unperturbed statistical equilibrium.

Remark. In the above introduction about the systems in (2.1) and (2.7), we only mention the continuous case with the full spectra. Nevertheless, the entire discussion can be directly applied to truncated systems with a Galerkin projection to finite number of spectral modes, which displays a more useful case for applications in various numerical simulations.

3. Statistical theories for truncated barotropic vorticity flows

In this section, we derive statistical properties for the barotropic equations (2.1) and fluctuation equations (2.7) through a general theoretical framework for a family of turbulent systems which has been used in many theoretical and applied developments about turbulent systems [23, 30, 11, 25]. The general statistical theories are developed in detail in a recent book by one of the authors [31]. Useful invariant measure under zero deterministic forcing and statistical energy dynamical equations are developed for the barotropic vorticity flow according to the general statistical theories, which can offer important tools in the construction of reduced-order methods in the following sections.

An overview of statistical theories for general turbulent systems with quadratic nonlinearity

We first introduce an abstract formulation about a family of general turbulent systems which can represent a large variety of dynamical systems including (2.1) and (2.7). Consider the stochastic differential equation (SDE) family with specific forms of linear damping and white noise random forcing introduced by a metric matrix $\Lambda \geq 0$

$$\frac{d\mathbf{u}}{dt} = B(\mathbf{u},\mathbf{u}) + L\mathbf{u} - d\Lambda\mathbf{u} + \mathbf{F} + \Lambda^{1/2}\sigma\dot{\mathbf{W}}, \quad \mathbf{u} \in \mathbb{R}^N. \tag{3.1}$$

The last three terms on the right hand side above represent the dissipation and forcing. Nonlinearity is introduced through the quadratic form $B(\mathbf{u},\mathbf{u})$ that conserves energy $\mathbf{u}\cdot B(\mathbf{u},\mathbf{u}) = 0$ and satisfies the Liouville property $\mathrm{div}_{\mathbf{u}} B(\mathbf{u},\mathbf{u}) = 0$, while L is a skew-symmetric operator so that $\mathbf{u}\cdot L\mathbf{u} = 0$. The dot-product is defined according to a proper metric from the conserved 'energy', $\mathbf{u}\cdot\mathbf{v} \equiv \sum_j w_j u_j v_j$. The parameter Λ satisfies $\Lambda \geq 0$ as a fixed positive definite matrix, and $\Lambda^{1/2}$ is the square root according to the properly defined inner-product. This system can reach an explicit Gaussian invariant measure in statistical steady state when no deterministic forcing is added, $\mathbf{F} = \mathbf{0}$. The following proposition can be found by a direct application of Fokker-Planck equation [31].

Proposition 1. *(Existence of Gaussian invariant measure) The turbulent system (3.1), associated with energy conserving nonlinearity and no deterministic forcing* $\mathbf{F} = \mathbf{0}$*, has a Gaussian invariant measure* $p_{\rm eq}$ *in statistical steady state with equipartition of energy in each component of* $\mathbf{u}$*,*

$$p_{\rm eq}(\mathbf{u}) = C^{-1}\exp\left(-\frac{1}{2}\sigma_{\rm eq}^{-2}\mathbf{u}\cdot\mathbf{u}\right), \tag{3.2}$$

with $\sigma_{\rm eq}^2 = \sigma^2/2d$ *defining the equilibrium energy level under the structural assumptions for (3.1) listed above.*

For completeness this proposition is proved in Appendix A. One point of special notice about the proposition is that the inner-product in $p_{\rm eq}$ should be defined according to the *conserved quantities* in the system. When non-zero deterministic forcing perturbations, $\delta\mathbf{F} \neq \mathbf{0}$, are exerted, the statistical distribution may divert from the equilibrium measure $p_{\rm eq}$ due to the nonlinear interactions. An advantage of getting this Gaussian invariant measure $p_{\rm eq}$ in (3.2) is that linear response theory and fluctuation-dissipation theorem (FDT) can be applied directly with explicit forms in predicting first-order responses in statistics.

Linear response theory and FDT

The linear response theory and fluctuation-dissipation theory (FDT) offer a convenient way to get leading-order linear approximation about model responses to perturbations [17, 6, 32]. A strategy using FDT in capturing low-frequency climate variability of simple barotropic truncated model has been discussed in [20]. Consider the general unperturbed system (3.1), $\mathbf{F} = \mathbf{0}$, with invariant measure $p_{\rm eq}(\mathbf{u})$, and an external forcing perturbation in separation with temporal and spatial variables,

$$\delta\mathbf{F}(\mathbf{u}, t) = \mathbf{a}(\mathbf{u})\,\delta f(t).$$

The equilibrium statistics and leading-order correction to the perturbation of some functional about the state variable $A(\mathbf{u})$ can be formulated as an asymptotic expansion, $\langle A(\mathbf{u})\rangle = \langle A(\mathbf{u})\rangle_{\rm eq} + \delta\langle A(\mathbf{u})\rangle(t) + O\left(\delta^2\right)$, with

$$\langle A(\mathbf{u})\rangle_{\rm eq} = \int A(\mathbf{u})\, p_{\rm eq}(\mathbf{u})\, d\mathbf{u}, \quad \delta\langle A(\mathbf{u})\rangle(t) = \int_0^t \mathcal{R}_A(t-s)\,\delta f(s)\, ds. \tag{3.3}$$

Above the pointed-bracket denotes the statistical average under the solution from Fokker-Planck equation. $\mathcal{R}_A(t)$ is the *linear response operator* according to the functional A, which is calculated through correlation functions in the unperturbed climate only

$$\mathcal{R}_A(t) = \langle A[\mathbf{u}(t)]\, B[\mathbf{u}(0)]\rangle_{\rm eq}, \quad B(\mathbf{u}) = -\frac{\mathrm{div}_{\mathbf{u}}\left(\mathbf{a}p_{\rm eq}\right)}{p_{\rm eq}}. \tag{3.4}$$

The noise in the equations is not needed for FDT to be valid, but is required to generate the smooth equilibrium measure for the linear response operator. Note that even though in general the linear response operator is difficult to calculate considering the complicated and unaccessible equilibrium distribution, the simple form of the invariant measure, $p_{\rm eq}$, in the previous setting makes it possible for the development of exact formulation about the FDT algorithm and linear response operator (see Appendix B for the explicit forms of the linear response operators in the barotropic equations using the Gaussian invariant measure).

General theory about the statistical energy conserving principle

The Gaussian invariant measure in (3.2) can only be reached with zero deterministic forcing $\mathbf{F} = \mathbf{0}$. In many situations, we are more interested in the system's responses to external forcing perturbations $\delta\mathbf{F} \neq 0$. With non-zero deterministic forcing, the distribution of the state variables may differ significantly from the unperturbed Gaussian distribution with complex higher-order statistics. In order to get the model sensitivity to perturbations, a statistical energy principle [23] is developed, with the help of which we can estimate about the total statistical energy structure. With detailed triad energy conservation symmetry (see [23, 31] for details), we can achieve the conservation principle for the statistical energy E:

Proposition 2. *(Statistical energy conservation principle) For any turbulent dynamical systems in (3.1), the total statistical energy, $E = \bar{E} + E' = \frac{1}{2}\bar{\mathbf{u}}\cdot\bar{\mathbf{u}} + \frac{1}{2}\mathrm{tr}R$, satisfies the dynamical equation*

$$\frac{dE}{dt} = \bar{\mathbf{u}}\cdot D\bar{\mathbf{u}} + \mathrm{tr}(DR) + \bar{\mathbf{u}}\cdot\mathbf{F} + Q_\sigma, \tag{3.5}$$

where $\bar{\mathbf{u}}$ is the statistical mean and R is the covariance matrix, $D = -d\Lambda$ is the damping operator and Q_σ is from the random forcing effect.

The barotropic system as well as the fluctuation equations described in Section 2 can both be categorized into this abstract formulation (3.1), and the quadratic nonlinearity due to the advection $\nabla^\perp\psi\cdot\nabla q$ can be shown from direct calculation satisfying all these required energy/enstrophy conservation, Liouville property, and triad symmetry (specifically these properties are checked for the truncated system with high wavenumber N, details can be found in [4, 2]). So next we derive the explicit forms about the invariant measure and the statistical energy equations based on the topographic barotropic flow and its fluctuation equations.

3.1. Invariant measure for barotropic flow with topography

We apply the general statistical theories described above to the barotropic flow with topography in (2.1) and (2.7). Consider the truncated spectral expansion of the state variables of interest with high wavenumber truncation N under standard Fourier basis $\mathbf{e}_\mathbf{k}=\exp(i\mathbf{k}\cdot\mathbf{x})$ due to the periodic boundary condition

$$\omega_N=\sum_{1\le|\mathbf{k}|\le N}\hat{\omega}_\mathbf{k}e^{i\mathbf{k}\cdot\mathbf{x}},\quad \psi_N=\sum_{1\le|\mathbf{k}|\le N}\hat{\psi}_\mathbf{k}e^{i\mathbf{k}\cdot\mathbf{x}}=-\sum_{1\le|\mathbf{k}|\le N}\frac{\hat{\omega}_\mathbf{k}}{|\mathbf{k}|^2}e^{i\mathbf{k}\cdot\mathbf{x}},$$

where ψ_N is the Galerkin truncated stream function, and $\omega_N=\nabla^2\psi_N$ is the truncated small-scale relative vorticity. The dynamical equations for the truncated spectral modes in both small and large scales can be derived by projecting the original equations (2.1) and (2.7) onto each spectral basis. It should be noticed that the truncated energy E_N and enstrophy $\mathscr{E}_N$ are still conserved under the system with Galerkin projection [4].

Damping and random noise forcing from pseudo-energy conservation

As described in the general theory, the invariant measure depends on the conserved quantities in the system, and the specific forms for the damping and random noise should be constructed according to the inner-product induced by the proper conserved quantity. We want to take into account both the conservation of energy and enstrophy. Therefore using the inner-product induced by the pseudo-energy $\tilde{E}$ in (2.8) should be a desirable choice for both topographic barotropic flow (2.1) and the equations about fluctuations (2.7). The damping and random noise added on the right hand sides of (2.1) and (2.7) consistent with the Gaussian invariant measure according to the pseudo-energy can be proposed in both small-scale and large-scale on each spectral mode as

$$\begin{aligned}&\text{A) Small}-\text{scale}\quad \begin{cases}-d\lambda_\mathbf{k}\left(\omega_\mathbf{k}-\bar{\omega}_{\text{eq},\mathbf{k}}\right)+\sigma_{1,\mathbf{k}}\lambda_\mathbf{k}^{1/2}\dot{W}_\mathbf{k},\\ -d\lambda_\mathbf{k}\left[(\omega_\mathbf{k}-\mu\psi_\mathbf{k})-\left(\bar{\omega}_{\text{eq},\mathbf{k}}-\mu\bar{\psi}_{\text{eq},\mathbf{k}}\right)\right]+\sigma_{2,\mathbf{k}}\lambda_\mathbf{k}^{1/2}\dot{W}_\mathbf{k}.\end{cases}\\ &\text{B) Large}-\text{scale}\quad -d\lambda_0\left(U-\bar{U}_{\text{eq}}\right)+\sigma\mu^{-1/2}\lambda_0^{1/2}\dot{W}_0.\end{aligned}\tag{3.6}$$

$(\lambda_0,\lambda_\mathbf{k})$ are the additional scaling parameters offering more freedom for specific applications; (d,σ) are the damping and noise parameters. Here two different dissipation forms are proposed for the small-scale vortical modes: i) the linear Ekman damping, $-d\omega$; ii) combined damping applied on the pseudo-energy induced quantity, $-d(\omega-\mu\psi)$. Both forms have practical meaning depending on the problems of interest, thus we would like to consider both cases in the numerical tests in the following sections. The noise amplitude is added according to the conserved pseudo-energy to make sure the convergence to the invariant measure, that is, $\sigma_{1,\mathbf{k}}=\sigma\left(1+\mu|\mathbf{k}|^{-2}\right)^{-1/2}$, $\sigma_{2,\mathbf{k}}=\sigma$. Together we assume the large and small scale mean states in the form according to the linear dependence in (2.6) under each spectra mode

$$\bar{U}_{\text{eq}}=-\frac{\beta}{\mu},\quad \bar{\psi}_{\text{eq},\mathbf{k}}=\frac{\hat{h}_\mathbf{k}}{\mu+|\mathbf{k}|^2}\quad \bar{\omega}_{\text{eq},\mathbf{k}}=-\frac{|\mathbf{k}|^2}{\mu+|\mathbf{k}|^2}\hat{h}_\mathbf{k}.\tag{3.7}$$

In (3.6) we actually apply the Fokker-Planck equation and Proposition 1 to the fluctuation part of the variables, $U'=U-\bar{U}$, $\omega'_\mathbf{k}=\omega_\mathbf{k}-\bar{\omega}_\mathbf{k}$, and the mean state is achieved through the linear relation between the vorticity and stream function as formulated in (3.7). The Gaussian invariant measure according to (3.2) thus can be derived as

$$p_{\text{eq}}(U,\omega)=C^{-1}\exp\left[-\frac{\mu}{2}\sigma_{\text{eq}}^{-2}\left(U-\bar{U}_{\text{eq}}\right)^2-\frac{1}{2}\sigma_{\text{eq}}^{-2}\sum\left(1+\frac{\mu}{|\mathbf{k}|^2}\right)\left(\omega_\mathbf{k}-\bar{\omega}_{\text{eq},\mathbf{k}}\right)^2\right],\quad \sigma_{\text{eq}}^2=\frac{\sigma^2}{2d}.\tag{3.8}$$

This is also the Gibbs measure given the average energy and enstrophy constraints [4]. It can be checked easily that $p_{\text{eq}}(U,\omega)$ is indeed the invariant measure in equilibrium through direct substitution into Fokker-Planck equation. We summarize the above result as the following corollary.

Corollary 3. *(Invariant measures under barotropic pseudo-energy) In the Barotropic dynamical flow (2.1) as well as the fluctuation equation (2.7) with damping and noises according to the pseudo-energy (3.6), the invariant measure is Gaussian in the form (3.8) with mean state defined by* $\bar{U}_{\rm eq} = -\frac{\beta}{\mu}$, $\bar{\psi}_{{\rm eq},\mathbf{k}} = \frac{\hat{h}_{\mathbf{k}}}{\mu+|\mathbf{k}|^2}$. *And the energy in each mode is determined by the energy partition rate* $\sigma^2_{\rm eq} = \frac{\sigma^2}{2d}$.

The next question is how the distributions about the state variables of interest differ from the above Gaussian invariant measure $p_{\rm eq}$ when (inhomogeneous) external forcing perturbations, $\delta\mathbf{F} = (\delta F_0, \delta F_{\mathbf{k}})$, are exerted on both small and large scale components. Note that even the unperturbed equilibrium measure is Gaussian, the perturbed distributions may divert largely with important skewness and kurtosis due to the nonlinear interactions inside the model. Still the linear response theory in (3.3) offers the convenience to get leading order approximations of the model responses using only unperturbed statistics in $p_{\rm eq}$. Furthermore, the explicit formulation of the invariant measure (3.8) makes it easy to calculate the linear response operator from (3.4) without any approximation errors. However the linear response theory as well as FDT can only offer linear approximations when the perturbation amplitude is infinitesimal, which will lead to large errors as the perturbation amplitude increases (see Figure 5.2 in Section 5.1.2 as an example). Then to investigate these nonlinear responses, let's first check the dynamics of the total statistical energy through the conserved quantities. The statistical energy principle offer the overall system response through one simple scalar equation and can be instructive about the system's energy structure as the responses become nonlinear. This is a guideline for the reduced models developed in Section 4.

3.2. Statistical energy principles for the barotropic flow system

Here we discuss the model responses in total statistical energy in the presence of external forcing perturbation and dissipation. With non-zero external forcing perturbations, the Gaussian invariant measure $p_{\rm eq}$ is no longer valid for the perturbed system. On the other hand, Proposition 2 tells that the dynamics of total statistical energy can be achieved through solving a simple scalar equation. Consider the statistical ensemble mean and disturbance about the mean state of the state variables of interest

$$U = \bar{U} + U', \quad \psi_{\mathbf{k}} = \bar{\psi}_{\mathbf{k}} + \psi'_{\mathbf{k}}.$$

The statistical energy E considers the combined energy in the mean and the variance in the disturbance about the mean state. Note that above the ensemble mean states $\left(\bar{U}, \bar{\psi}_{\mathbf{k}}\right)$ should be different from the unperturbed time-averaged mean $\left(\bar{U}_{\rm eq}, \bar{\psi}_{{\rm eq},\mathbf{k}}\right)$ in equilibrium (2.6) due to the deterministic forcing applied on the mean states. Again the triad symmetry required is guaranteed to be satisfied since the barotropic triad will always includes components, $\psi_{\mathbf{k}}, \psi_{\mathbf{m}}, \psi_{\mathbf{n}}$, with the selection rule, $\mathbf{k}+\mathbf{m}+\mathbf{n} = \mathbf{0}$ [2]. Thus the nonlinear terms make no contributions in the changes of total statistical energy. Below we consider the statistical energy equations individually for the original barotropic flow and the corresponding fluctuation equations. And here and after 'energy' is always referred in the general sense as some proper conserved quantity.

3.2.1. Barotropic flow with topography in periodic domain

In Section 2.1 we have shown that there exist two important conserved quantities, that is, the total mean energy, E, and the large-scale enstrophy, $\mathscr{E}$, in the topographic barotropic system. Thus two sets of corresponding statistical energy equations can be developed. The result from Proposition 2 can be applied directly.

Define the statistical energy from the total energy $E^{\rm ene}$, and the statistical energy form the enstrophy $E^{\rm ens}$ in the presence of dynamical mean flow $U(t)$ as

$$\begin{aligned} E^{\rm ene} &= \sum E^{\rm ene}_{\mathbf{k}} \equiv \frac{1}{2}\left(\bar{U}^2 + \overline{U'^2}\right) + \frac{1}{2}\sum_{\mathbf{k}\neq 0} |\mathbf{k}|^2 \left(\left|\bar{\psi}_{\mathbf{k}}\right|^2 + \overline{\left|\psi'_{\mathbf{k}}\right|^2}\right), \\ E^{\rm ens} &= \sum E^{\rm ens}_{\mathbf{k}} \equiv \beta\bar{U} + \frac{1}{2}\sum_{\mathbf{k}\neq 0}\left(\left|-|\mathbf{k}|^2\bar{\psi}_{\mathbf{k}} + \hat{h}_{\mathbf{k}}\right|^2 + |\mathbf{k}|^4\overline{\left|\psi'_{\mathbf{k}}\right|^2}\right). \end{aligned} \tag{3.9}$$

The 'overbar' in the above definitions can be viewed as ensemble averages for the mean and variance. $E^{\rm ene}_{\mathbf{k}}, E^{\rm ens}_{\mathbf{k}}$ represent the statistical energy and enstrophy in each spectral mode $\mathbf{k}$ ($\mathbf{k} = 0$ represents the large-scale mode U), that

combine the energy in the mean and variance. The summation above could be taken among all the resolved truncated modes, $1 \le |\mathbf{k}| \le N$. The dynamical equations for the **generalized statistical energy E^{ene} and enstrophy equations E^{ens} including a mean flow** $U(t)$ for the barotropic flow (2.1) can be derived according to the abstract formulation (3.5)

$$\begin{aligned}\frac{dE^{\text{ene}}}{dt} &= -2\sum_{\mathbf{k}\neq 0}\mathcal{D}_{\mathbf{k}}E^{\text{ene}}_{\mathbf{k}} - 2\mathcal{D}_0E^{\text{ene}}_0 - \langle\bar{\psi},F\rangle + \bar{U}F_0 + Q^{\text{ene}}_{\sigma},\\ \frac{dE^{\text{ens}}}{dt} &= -2\sum_{\mathbf{k}\neq 0}\mathcal{D}_{\mathbf{k}}E^{\text{ens}}_{\mathbf{k}} - \mathcal{D}_0E^{\text{ens}}_0 + \langle\bar{q},\mathcal{D}h+F\rangle + \beta F_0 + Q^{\text{ens}}_{\sigma}.\end{aligned} \tag{3.10}$$

with the damping and noise operators defined from the spectral representation of the original damping $\mathcal{D}$ as

$$\mathcal{D}_{\mathbf{k}} = \sum_{l=0}^{L} d_l\,|\mathbf{k}|^{2l-2}, \quad \mathcal{D}h = \sum_{\mathbf{k}\neq 0}\mathcal{D}_{\mathbf{k}}\hat{h}_{\mathbf{k}};$$

$$Q^{\text{ene}}_{\sigma} = \frac{1}{2}\sum_{\mathbf{k}\neq 0}|\mathbf{k}|^{-2}\,Q_{\sigma,\mathbf{k}} + Q_{\sigma,U}, \quad Q^{\text{ens}}_{\sigma} = \frac{1}{2}\sum_{\mathbf{k}\neq 0}Q_{\sigma,\mathbf{k}};$$

the mean potential vorticity $\bar{q} = \sum \bar{q}_{\mathbf{k}}e^{i\mathbf{k}\cdot\mathbf{x}} = \sum\left(-|\mathbf{k}|^2\,\bar{\psi}_{\mathbf{k}} + \hat{h}_{\mathbf{k}}\right)e^{i\mathbf{k}\cdot\mathbf{x}}$; and inner-product in pointed-bracket

$$\langle f,g\rangle = \oint fg = \sum \hat{f}_{\mathbf{k}}\hat{g}^{*}_{\mathbf{k}}.$$

On the right hand sides of the equations (3.10), the first two parts represent the damping effects on both the small and large scales in the general sense. With the specific form of the uniform damping terms in (3.6), the statistical energy equations (3.10) can be further simplified with a uniform damping for the total energy or enstrophy, $-dE$, instead of the selective damping for each mode, $E_{\mathbf{k}}$, which will make the equations even easier to solve in applying to numerical methods. The last three parts show the energy/enstrophy sources from external forcing in both deterministic and stochastic components. Note only the first-order moments of the mean are included in the deterministic forcing effects with $\langle\bar{\psi},F\rangle$ or $\langle\bar{q},F\rangle$ for the energy and enstrophy statistical changes. One additional term $\langle\bar{q},\mathcal{D}h\rangle$ is included in the statistical enstrophy equation representing the topographic stress. Instability and chaotic structure can be generated through the topographic stress due to the positive eigenvalues introduced in this interaction as an additional forcing effect. One advantage of the statistical energy equations is that we can predict the total responses of second-order moments from E^{ene} or E^{ens} with only knowledge of first-order moments required in the dynamics [4, 11].

3.2.2. Fluctuation equations of the topographic barotropic flow

In the fluctuation equations (2.7), neither energy nor enstrophy will stay conserved any longer. However we can find another conserved quantity (2.8) as a linear combination between the energy and enstrophy. Define the statistical pseudo-energy by the combination of statistical energy E^{ene} and enstrophy E^{ens}

$$E^{\text{stat}} = E^{\text{ens}} + \mu E^{\text{ene}} = \frac{\mu}{2}\left(\bar{U}^2 + \overline{U'^2}\right) + \frac{1}{2}\sum_{\mathbf{k}\neq 0}\left(1+\mu\,|\mathbf{k}|^{-2}\right)\left(|\bar{\omega}_{\mathbf{k}}|^2 + \overline{\left|\omega'_{\mathbf{k}}\right|^2}\right). \tag{3.11}$$

Here both the small and large scale variables in (3.11) should be viewed as the fluctuation parts $\left(\tilde{U},\tilde{\omega}_{\mathbf{k}}\right)$ about the unperturbed mean as in (2.5). Especially in the case $\mu < -1$, instabilities can be introduced in modes $|\mathbf{k}|^2 < -\mu$. In the fluctuation equations (2.7), still the nonlinear interactions conserve the pseudo-energy $\tilde{E}$ and the triad symmetry is guaranteed with the same reason as the previous case. The additional concern for the development of statistical energy dynamics comes from the inclusion of interactions terms with the mean states, $\nabla^{\perp}\bar{\psi}_{\text{eq}}\cdot\nabla(\omega-\mu\psi)$ and $\frac{\partial\bar{q}_{\text{eq}}}{\partial x}U$. Again it can be proved that these linear terms are skew-symmetric and do not alter the total statistical pseudo-energy structure [4].

The **dynamical equation for the generalized statistical pseudo-energy E^{stat} with dissipation and external forcing** becomes

$$\frac{dE^{\text{stat}}}{dt} = -2\sum_{\mathbf{k}\neq 0}\mathcal{D}_{\mathbf{k}}E^{\text{stat}}_{\mathbf{k}} - 2\mathcal{D}_0E^{\text{stat}}_0 + \langle\bar{\omega}-\mu\bar{\psi},F\rangle + \mu\bar{U}F_0 + Q_{\sigma}. \tag{3.12}$$

Again we use the pointed-bracket to include the contribution from the forced modes though interaction with the statistical mean

$$\langle \bar{\omega} - \mu\bar{\psi}, F \rangle = \oint (\bar{\omega}_\Lambda - \mu\bar{\psi}_\Lambda) F = \sum_{\mathbf{k}\neq 0} \left(1 + \mu |\mathbf{k}|^{-2}\right) \hat{F}^*_{\mathbf{k}} \bar{\omega}_{\mathbf{k}}.$$

And the entire contribution from random forcing in both small and large scales becomes

$$Q_\sigma = Q^{\text{ens}}_\sigma + \mu Q^{\text{ene}}_\sigma = \frac{1}{2} \sum_{\mathbf{k}\neq 0} \left(1 + \mu |\mathbf{k}|^{-2}\right) Q_{\sigma,\mathbf{k}} + \mu Q_{\sigma,U}.$$

Like the previous case, with the uniform damping terms in (3.6) the first two terms on the right hand side of (3.12) will become homogeneous, $-dE^{\text{stat}}$. The rest parts on the right hand side represent the energy injected into the system through the deterministic and stochastic forcing. Note again that only the first-order mean statistics are needed in the statistical dynamics to achieve the total energy structure.

4. Reduced-order statistical methods for principal responses

In this section, we discuss the central issue of this paper about the development of reduced-order methods to capture model sensitivity to external perturbations combining the mathematical theories described above. The basic idea is following [11] in constructing low-dimensional statistical closure models that have the skill in i) maintaining equilibrium consistency in unperturbed system; ii) capturing the model responses in principal directions to various external forcing perturbations. The finite-dimensional truncation of the barotropic equations in (2.1) is obtained by making a Galerkin approximation where the equations are projected into a subspace with high wavenumber truncation. Consider the Galerkin projection operator $\mathcal{P}_N$ on a subspace with wavenumbers $1 \leq |\mathbf{k}| \leq N$, $\mathcal{P}_N (U(t), \psi(\mathbf{x}, t)) = (U(t), \psi_N(\mathbf{x}, t))$, applied to the true model for topographic barotropic flow (2.1) with the specific forcing and Ekman damping terms defined in (3.6)

$$\begin{aligned}
\frac{d\omega_{\mathbf{k}}}{dt} &= \mathcal{P}_{N,\mathbf{k}} \left(\nabla^\perp \psi_N \cdot \nabla q_N\right) + ik_x \left(\beta / |\mathbf{k}|^2 - U\right) \omega_{\mathbf{k}} - ik_x \hat{h}_{\mathbf{k}} U \qquad (4.1a)\\
&\quad -d\omega_{\mathbf{k}} + \sigma_{\mathbf{k}} \dot{W}_{\mathbf{k}} + \hat{F}_{\mathbf{k}} + \delta \hat{F}_{\mathbf{k}}, \qquad 1 \leq |\mathbf{k}| \leq N,\\
\frac{dU}{dt} &= \sum_{1\leq|\mathbf{k}|\leq N} \frac{ik_x}{|\mathbf{k}|^2} \hat{h}^*_{\mathbf{k}} \omega_{\mathbf{k}} - dU + \sigma_0 \dot{W}_0 + F_0 + \delta F_0. \qquad (4.1b)
\end{aligned}$$

The stochastic noise is defined in each mode, $\sigma_0 = \sigma\mu^{-1/2}$, $\sigma_{\mathbf{k}} = \sigma \left(1 + \mu / |\mathbf{k}|^2\right)^{-1/2}$. The damping and noise terms are added according to (3.6) to reach the Gaussian invariant measure (3.8) in unperturbed case $\delta \hat{F}_{\mathbf{k}} = 0, \delta F_0 = 0$. The deterministic forcing is introduced in consistency with the climatology from (3.7)

$$\hat{F}_{\mathbf{k}} = d\bar{\omega}_{\text{eq},\mathbf{k}}, \quad F_0 = d\bar{U}_{\text{eq},\mathbf{k}}.$$

In a similar fashion, we can write down the formulations with other damping forms and the fluctuation equations as in (3.6). Without loss of generality, we will focus on the equations in the form of (4.1) in this section and discuss the construction of reduced-order methods based on this model.

We first discuss the formulation of the exact statistical moment dynamics. And then the reduced-order models are introduced through a careful calibration about the ignored nonlinear interaction terms from the unresolved mode in $\mathcal{P}_N (\nabla^\perp \psi_N \cdot \nabla q_N)$. Specifically, we need to consider the statistical dynamics of large and small scale mean $\left(\bar{U}, \bar{\psi}_{\mathbf{k}}\right)$, and the covariances $\left(\overline{U'^2}, \overline{U'\psi'_{\mathbf{k}}}, \overline{\left|\psi'_{\mathbf{k}}\right|^2}\right)$ in both small and large scale components, as well as the total statistical energy E^{stat} in the reduced-order models. The model parameters are tuned in a training phase in a systematic way under proper information metric with the help of linear response theory, and the imperfect models' optimal skill in capturing the responses to different perturbation amplitude is checked in different dynamical regimes.

4.1. Formulation of the exact statistical moment dynamics

4.1.1. Exact dynamics for the statistical mean

The mean dynamical equations for the large and small state variables $\left(\bar{U}, \bar{\psi}_{\mathbf{k}}\right)$ in (4.1) can be achieved by taking probabilistic expectation on both sides of the equations

$$\begin{aligned} \frac{d\bar{\psi}_{\mathbf{k}}}{dt} + Q_{\psi,\mathbf{k}} + L_{m,\mathbf{k}} &= -d\bar{\psi}_{\mathbf{k}} + \hat{F}_{\mathbf{k}} + \delta\hat{F}_{\mathbf{k}}, \\ \frac{d\bar{U}}{dt} - i\sum k_x \hat{h}^*_{\mathbf{k}} \bar{\psi}_{\mathbf{k}} &= -d\bar{U} + F_0 + \delta F_0. \end{aligned} \tag{4.2}$$

In the mean dynamics, the left hand side of the small-scale equations for $\bar{\psi}_{\mathbf{k}}$ shows the quadratic interaction term as well as the skew-symmetric forms from β-effect and topography; topographic stress on the mean state applies on the left hand side of the large-scale mean flow $\bar{U}$. Only linear damping and deterministic forcing terms will appear on the right hand side of the equations and the random forcing terms have mean zero and vanish in mean equations. Especially in small-scale dynamics, Q_ψ is the cross-interactions between modes of different scales and L_m represents the quasi-linear part as well as the large-small scale interaction

$$\begin{aligned} Q_{\psi,\mathbf{k}} &= \sum_{\mathbf{m}} \frac{\mathbf{k}^\perp \cdot \mathbf{m}}{|\mathbf{k}|^2} \left[|\mathbf{m}|^2 \left(\bar{\psi}_{\mathbf{m}} \bar{\psi}_{\mathbf{k}-\mathbf{m}} + \overline{\psi'_{\mathbf{m}} \psi'_{\mathbf{k}-\mathbf{m}}} \right) - \hat{h}_{\mathbf{m}} \bar{\psi}_{\mathbf{k}-\mathbf{m}} \right], \\ L_{m,\mathbf{k}} &= ik_x \left(\bar{U} \bar{\psi}_{\mathbf{k}} + \overline{U' \psi'_{\mathbf{k}}} \right) - ik_x |\mathbf{k}|^{-2} \left(\hat{h}_{\mathbf{k}} \bar{U} + \beta \bar{\psi}_{\mathbf{k}} \right). \end{aligned}$$

Second-order moments interact with the mean dynamics through the cross-covariances, $\overline{\psi'_{\mathbf{m}} \psi'_{\mathbf{k}-\mathbf{m}}}$ and $\overline{U' \psi'_{\mathbf{k}}}$, in the above terms Q_ψ and L_m. Thus the first-order mean dynamics (4.2) are not a closed system yet and the fluctuations about the mean can affect the mean structure through these second-order feedbacks from the dynamics.

4.1.2. Exact dynamics for the covariance

The covariance dynamical equations involve the evolution of the variances in both small and large scale variables as well as their cross-covariance, $\left(r_U, c_{U\psi,\mathbf{k}}, r_{\psi,\mathbf{k}}\right) \equiv \left(\overline{U'^2}, \overline{U' \psi'_{\mathbf{k}}}, \overline{\left|\psi'_{\mathbf{k}}\right|^2}\right)$. The dynamics can be derived as

$$\begin{aligned} \frac{dr_{\psi,\mathbf{k}}}{dt} + 2L_{r,\mathbf{k}} + 2Q_{\psi\psi,\mathbf{k}} &= -2dr_{\psi,\mathbf{k}} + |\mathbf{k}|^{-2} \sigma^2_{\mathbf{k}}, \\ \frac{dr_U}{dt} + 2\Im\mathfrak{m} \sum k_x \hat{h}^*_{\mathbf{k}} c_{U\psi,\mathbf{k}} &= -2dr_U + \mu^{-1}\sigma^2, \\ \frac{dc_{U\psi,\mathbf{k}}}{dt} + L_{c,\mathbf{k}} + Q_{U\psi,\mathbf{k}} &= -2dc_{U\psi,\mathbf{k}}. \end{aligned} \tag{4.3}$$

where the small-scale random forcing $\sigma^2_{\mathbf{k}} = \left(\mu + |\mathbf{k}|^2\right)^{-1} \sigma^2$ applies on each mode as a source of fluctuation and $\mu^{-1}\sigma^2$ serves as random forcing on large-scale mean flow fluctuations. The deterministic forcing is cancelled on the right hand side of the equations, while the random forcing terms apply on the variances. We assume the random forcing is independent white noise in small and large scales thus the covariance $c_{U\psi}$ is not forced. Note that $c_{U\psi}$ will stay zero in the unperturbed case according to the Gaussian invariant measure (3.8) derived in Section 3.1, while it becomes crucial as perturbations $\delta F \neq 0$ are applied. Thus the accurate approximation about the cross-covariance term in response to perturbations play an important role in the construction of the reduced-order models. L_r and L_c represent the quasi-linear effects between the small and large scale variables, while $Q_{\psi\psi}$ and $Q_{U\psi}$ include the higher-order statistics and cross-covariances representing the nonlinear triad interactions between modes $\mathbf{k} = \mathbf{m} + \mathbf{n}$ in different scales

$$\begin{aligned} L_{r,\mathbf{k}} &= -k_x \Im\mathfrak{m}\left(\bar{\psi}_{\mathbf{k}} c^*_{U\psi,\mathbf{k}}\right) + k_x |\mathbf{k}|^{-2} \Im\mathfrak{m}\left(\hat{h}_{\mathbf{k}} c^*_{U\psi,\mathbf{k}}\right), \\ L_{c,\mathbf{k}} &= ik_x \left(\bar{\psi}_{\mathbf{k}} - \hat{h}_{\mathbf{k}} |\mathbf{k}|^{-2}\right) r_U + ik_x \left(\bar{U} - \beta |\mathbf{k}|^{-2}\right) c_{U\psi,\mathbf{k}} - i \sum m_x \hat{h}_{\mathbf{m}} \overline{\psi^*_{\mathbf{m}} \psi_{\mathbf{k}}}. \end{aligned}$$

$$Q_{\psi\psi,\mathbf{k}} = \sum \frac{\mathbf{k}^\perp \cdot \mathbf{m}}{|\mathbf{k}|^2}\left[|\mathbf{m}|^2\left(\bar{\psi}_{\mathbf{m}}\overline{\psi'_{\mathbf{k}-\mathbf{m}}\psi'^*_{\mathbf{k}}} + \bar{\psi}_{\mathbf{k}-\mathbf{m}}\overline{\psi'_{\mathbf{m}}\psi'^*_{\mathbf{k}}} + \overline{\psi'_{\mathbf{m}}\psi'_{\mathbf{k}-\mathbf{m}}\psi'^*_{\mathbf{k}}}\right) - \hat{h}_{\mathbf{m}}\overline{\psi'_{\mathbf{k}-\mathbf{m}}\psi'^*_{\mathbf{k}}}\right],$$

$$Q_{U\psi,\mathbf{k}} = \sum \frac{\mathbf{k}^\perp \cdot \mathbf{m}}{|\mathbf{k}|^2}\left[|\mathbf{m}|^2\left(\bar{\psi}_{\mathbf{m}}\overline{U'\psi'_{\mathbf{k}-\mathbf{m}}} + \bar{\psi}_{\mathbf{k}-\mathbf{m}}\overline{U'\psi'_{\mathbf{m}}} + \overline{U'\psi'_{\mathbf{m}}\psi'_{\mathbf{k}-\mathbf{m}}}\right) - \hat{h}_{\mathbf{m}}\overline{U'\psi'_{\mathbf{k}-\mathbf{m}}}\right] + ik_x\overline{U'U'\psi'_{\mathbf{k}}}.$$

On the left hand side of (4.3), the skew-symmetric linear operators including mean flow $\bar{U}$ and β-effect make no contribution in the variance dynamics in $\left(r_U, r_\psi\right)$. The third-moments between U and $\psi_{\mathbf{k}}$ only appear in the cross-covariance dynamics about $c_{U\psi}$ through the term $Q_{U\psi}$. On the other hand, the dynamical equations for the cross-covariance, $c_{U\psi}$, contains the contributions from the large and small scale variances as well as the higher order moments, $\overline{U'U'\psi'_{\mathbf{k}}}$, in the last term. Therefore, the changes in mean states $\left(\bar{U}, \bar{\psi}\right)$ due to deterministic forcing perturbation will first activate the cross-covariance, $c_{U\psi}$; $c_{U\psi}$ represents energy transfers between small and large scales and will finally affect the energy structure in variances $\left(r_U, r_\psi\right)$ through topographic stress and higher-order statistics.

4.2. Low-dimensional reduced-order closure models

In developing reduced-order models, we may concentrate on the first M dominant modes, $|\mathbf{k}| \le M, M \ll N$, that often contain the largest amount of energy in the system. The nonlinear term in (4.1) always involves interactions between modes in a wide spectra through the triads $\mathbf{k} = \mathbf{m} + \mathbf{n}$. Thus the (unresolved) less energetic high wavenumber modes ($|\mathbf{k}| > M$) could be important for the final energy spectra in low wavenumber modes ($|\mathbf{k}| \le M$) due to the strong backward cascade of energy through these nonlinear triad interactions. Therefore careful calibration is required for the small-scale unresolved dynamical effects in the construction of low-dimensional truncated reduced-order models to achieve both computational accuracy and efficiency.

The basic idea can be viewed as replacing the expensive nonlinear interactions in the small-scale with proper additional damping and noise

$$\sum_{\mathbf{m}} \frac{\mathbf{k}^\perp \cdot \mathbf{m}}{|\mathbf{k}|^2}\psi_{\mathbf{k}-\mathbf{m}}\left(\psi_{\mathbf{m}} - \hat{h}_{\mathbf{m}}\right) \to -\left(d_{M,\mathbf{k}} + i\omega_{M,\mathbf{k}}\right)\psi_{M,\mathbf{k}} + \sigma_{M,\mathbf{k}}\dot{W}_{M,\mathbf{k}} + G_{M,\mathbf{k}}.$$

Besides, similar correction terms $-d_{M,0}U_M + \sigma_{M,0}\dot{W}_{M,0} + H_M$ are introduced for the large-scale dynamics for further corrections of the errors in the large-scale mean flow. Imperfect model parameters $(d_M, \omega_M, \sigma_M)$ are introduced for correcting the unresolved effects. The linear damping and Gaussian random noise, $-\left(d_{M,\mathbf{k}} + i\omega_{M,\mathbf{k}}\right)\psi_{M,\mathbf{k}} + \sigma_{M,\mathbf{k}}\dot{W}_{M,\mathbf{k}}$, are used to correct error from the unresolved nonlinear interactions, $\psi_{\mathbf{k}}\psi_{\mathbf{k}-\mathbf{m}}$. Additional damping serves as the stabilizing effects balancing on the linearly unstable modes, and adding additional white stochastic excitation models the energy received on the stable modes [22, 21]. One further correction term $G_{M,\mathbf{k}}$ is used to correct the unresolved interactions between $\psi_{\mathbf{m}}\hat{h}_{\mathbf{k}-\mathbf{m}}$ in the topographic structure and maintains climate consistency in the imperfect approximation.

Equivalently, in the reduced-order statistical dynamics the higher-order nonlinear interactions are replaced by the corrections above accordingly. Therefore we can derive the **dynamics for the statistical mean and variances in imperfect reduced-order closure models**:

- *mean equations*:

$$\begin{aligned} \frac{d\bar{\psi}_{\mathbf{k}}}{dt} + L_{m,\mathbf{k}} &= -d\bar{\psi}_{\mathbf{k}} + \hat{F}_{\mathbf{k}} + \delta\hat{F}_{\mathbf{k}} \underline{-\left(d_{M,\mathbf{k}} + i\omega_{M,\mathbf{k}}\right)\bar{\psi}_{\mathbf{k}} + G_{M,\mathbf{k}}}, \\ \frac{d\bar{U}}{dt} - \sum ik_x\hat{h}^*_{\mathbf{k}}\bar{\psi}_{\mathbf{k}} &= -d\bar{U} + F_0 + \delta F_0 \underline{-d_{M,0}\bar{U} + H_M}. \end{aligned} \tag{4.4}$$

- *covariance equations*:

$$\begin{aligned} \frac{dr_{\psi,\mathbf{k}}}{dt} + 2L_{r,\mathbf{k}} &= -2dr_{\psi,\mathbf{k}} + |\mathbf{k}|^{-2}\sigma^2_{\mathbf{k}} \underline{-2d_{M,\mathbf{k}}r_{\psi,\mathbf{k}} + \sigma^2_{M,\mathbf{k}}}, \\ \frac{dr_U}{dt} + 2\Im\mathfrak{m}\sum k_x\hat{h}^*_{\mathbf{k}}c_{U\psi,\mathbf{k}} &= -2dr_U + \mu^{-1}\sigma^2 \underline{-2d_{M,0}r_U + \sigma^2_{M,0}}, \\ \frac{dc_{U\psi,\mathbf{k}}}{dt} + L_{c,\mathbf{k}} &= -2dc_{U\psi,\mathbf{k}} \underline{-\left(d_{M,0} + d_{M,\mathbf{k}} + i\omega_{M,\mathbf{k}}\right)c_{U\psi,\mathbf{k}}}. \end{aligned} \tag{4.5}$$

The above equations are only solved for the first few resolved modes among wavenumbers $1 \le |\mathbf{k}| \le M$. The underlined parts are the additional terms introduced for correction of the imperfect reduced-order models. Among the parameters, $d_{M,\mathbf{k}}$ is the additional damping to stabilize the unstable modes with positive Lyapunov exponents; $\omega_{M,\mathbf{k}}$ characterizes the communication between the large and small scales in the covariance $c_{U\psi}$; $\sigma_{M,\mathbf{k}}$ is the additional noise to compensate for the overdamped stable modes; while (G_M, H_M) are additional corrections that can be calculated from the steady state information in the unperturbed system. Comparing the reduced-order closure models (4.4)-(4.5) with the original exact system (4.2)-(4.3), the additional corrections are used for approximating both the higher-order moments (like $\underline{\overline{\psi'_{\mathbf{m}}\psi'_{\mathbf{k}-\mathbf{m}}\psi'^{*}_{\mathbf{k}}}}$ from $Q_{\psi\psi}$) and the unresolved second-order covariances (like $\underline{\overline{\psi'_{\mathbf{m}}\psi'_{\mathbf{k}-\mathbf{m}}}}$ from Q_{ψ}) in the unresolved high wavenumber modes. Next the central task is to find proper ways to propose the parameter values, which i) recover the equilibrium statistics in the unperturbed case; and ii) capture the most important statistical sensitivity when the system is perturbed. Note that these parameters will eventually depend on the total statistical energy (see (4.6)-(4.10) below).

4.2.1. Climate consistency

In the first place, we need to make sure the imperfect models' consistency with the unperturbed climate of the true system. That is, the same final unperturbed statistical equilibrium can be recovered from the reduced-order models. The corrections for the statistical mean dynamics (G_∞, H_∞) can be first estimated from the equilibrium statistics (climate) from (4.4). In particular we derive the equilibrium equations

$$\begin{aligned} &L_{m,\mathbf{k},\mathrm{eq}} - \hat{F}_{\mathbf{k}} + (d + d_{M,\mathbf{k}} + i\omega_{M,\mathbf{k}})\,\bar{\psi}_{\mathbf{k},\mathrm{eq}} = G_{\infty,\mathbf{k}}, \\ &-\sum ik_x \hat{h}^*_{\mathbf{k}} \bar{\psi}_{\mathbf{k},\mathrm{eq}} - F_0 + (d + d_{M,0})\,\bar{U}_{\mathrm{eq}} = H_\infty. \end{aligned} \tag{4.6}$$

Above $L_{m,\mathrm{eq}}$ can be calculated from the equilibrium information of $\bar{U}_{\mathrm{eq}}, \bar{\psi}_{\mathbf{k},\mathrm{eq}}$ as well as the covariance $\overline{U'\psi'_{\mathbf{k}}}_{\mathrm{eq}}$ (which should be zero in the unperturbed steady state). The above constraints (4.6) guarantee that the imperfect reduced-order system converges to this true climate statistics in the mean state. Similarly we can find the first estimations about the additional damping and noise parameters $(d_{M,\mathbf{k}}, \sigma_{M,\mathbf{k}})$ through the equilibrium statistics from (4.5). For simplicity, we assume the additional damping coefficients are only constant scaled with the equilibrium statistics among all the resolved modes, $d_{M,\mathbf{k}} = \epsilon r^{-1}_{\mathbf{k},\mathrm{eq}}$, with $\epsilon > 0$ a constant controlling the additional damping rate. The additional noises, $\sigma^2_{M,\mathbf{k}}$, then can be calculated accordingly from the equilibrium equations of (4.5). In the unperturbed case with Gaussian invariant measure for the system (4.1), the constraints of climate consistency become much simpler, that is,

$$d_{M,\mathbf{k}} = \epsilon r^{-1}_{\mathbf{k},\mathrm{eq}}, \quad \sigma^2_{M,\mathbf{k}} = 2 d_{M,\mathbf{k}} r_{\mathbf{k},\mathrm{eq}}, \quad \epsilon > 0. \tag{4.7}$$

By choosing parameters according to (4.6) and (4.7), the climate consistency for the imperfect reduced-order models in (4.4) and (4.5) in the unperturbed equilibrium is guaranteed. In addition, we still have one controlling parameter ϵ for the freedom to tune the imperfect model performance, considering that climate consistency is only the necessary but not sufficient condition for good model prediction [15].

4.2.2. Model sensitivity

Here we want to find a unified way to achieve the optimal model parameters $(d_{M,\mathbf{k}}, \omega_{M,\mathbf{k}})$ such that the imperfect models can reach optimal performance for various kinds of external perturbations. In general the imperfect models may still be far from optimal even though the climate consistency is guaranteed from the previous step. Accurate modeling about the model sensitivity to various external perturbation forms requires the imperfect reduced-order models to correctly reflect the true system's "memory" to its previous states. Following the idea in [11], it is noticed that the linear response operator $\mathcal{R}_A$ in (3.4) can characterize the model sensitivity involving the nonlinear effects in the system regardless of the specific forms of the external perturbations. The optimal imperfect model parameter thus can be achieved when the linear response operator is recovered with best accuracy in the reduced models. Therefore the general reduced-order model algorithm is split into two separated steps of a training phase and a prediction phase. The training phase is used to improve model sensitivity by tuning the model parameter ϵ using only unperturbed climate statistics for the linear response operator. Then the optimal parameter can be applied for predicting the model responses to different kinds of external perturbations.

Information-theoretical framework to measure the linear responses. In this training phase, we try to find the optimal model parameter ϵ by comparing the linear response operators from the true system and imperfect approximation model. Thanks to the Gaussian invariant measure, we can calculate the true linear response operator of the system from the exact formulas (still numerical errors might be included in this truth due to the time-average of the third moments along a long trajectory); and the linear response operators from the reduced-order models can be calculated through the *kicked-response strategy* as we applied in [11]. The distance between these two operators can be calculated through the information metric from [33, 15] which offers an unbiased and invariant measure for model distributions

$$\begin{aligned}\mathscr{P}\left(\pi_\delta, \pi_\delta^M\right) &= \mathscr{S}\left(\pi_{G,\delta}\right) - \mathscr{S}\left(\pi_\delta\right) \\ &+\frac{1}{2}\sum_{\mathbf{k}} \left(\delta\bar{u}_{\mathbf{k}} - \delta\bar{u}_{M,\mathbf{k}}\right) R_{\mathbf{k}}^{-1} \left(\delta\bar{u}_{\mathbf{k}} - \delta\bar{u}_{M,\mathbf{k}}\right) \\ &+\frac{1}{4}\sum_{\mathbf{k}} R_{\mathbf{k}}^{-2} \left(\delta R_{\mathbf{k}} - \delta R_{M,\mathbf{k}}\right)^2 + O\left(\delta^3\right). \end{aligned} \tag{4.8}$$

The first row above is the inherent information barrier due to the second-order closure approximation; second row is the signal error from calibrating the linear responses in the mean, $\delta\bar{u}_{\mathbf{k}}$; and the last row is the dispersion error for calibrating the linear response in the second order moments, $\delta R_{\mathbf{k}}$.

Correction through total statistical energy. In this final step, we consider further improvement about the model sensitivity using the correction through total statistical energy from (3.10) or (3.12). In the above model calibrations both with climate consistency (4.6)-(4.7) and training model parameters under information metric (4.8), only unperturbed equilibrium statistics are used. To capture the responses to a specific perturbation forcing, it is better to make the imperfect model parameters change adaptively according to the total energy structure [11]. Then we propose the mean dynamics correction terms scaled with the total statistical energy E as

$$G_{M,\mathbf{k}} \to \left(\frac{E}{E_{\text{eq}}}\right) G_{\infty,\mathbf{k}}, \quad H_M \to \left(\frac{E}{E_{\text{eq}}}\right) H_\infty. \tag{4.9}$$

And the additional damping and noise can be taken with the scale as

$$d_{M,\mathbf{k}} r_{\mathbf{k}} \to \epsilon \left(\frac{E}{E_{\text{eq}}}\right)^{1/2} \frac{r_{\mathbf{k}}}{r_{\mathbf{k},\text{eq}}}, \quad \sigma_{M,\mathbf{k}}^2 \to 2\epsilon \left(\frac{E}{E_{\text{eq}}}\right)^{3/2}. \tag{4.10}$$

Above in (4.9) and (4.10), E is the statistical energy or enstrophy from (3.9) (or for the fluctuation equations, it is the statistical pseudo-energy in (3.11)). And E_{eq} is the unperturbed total statistical energy in equilibrium. For example, if the conserved total energy $E \equiv E^{\text{ene}}$ in (3.9) is applied, the statistical energy dynamics to solve in (3.10) can be simplified in the form

$$\frac{dE}{dt} = -2dE - \sum \bar{\psi}_{\mathbf{k}}^* \delta\hat{F}_{\mathbf{k}} + \bar{U}\delta F_0 + Q_E. \tag{4.11}$$

Only perturbed mean modes are required on the right hand side for solving the total statistical energy structure in response, and Q_E contains all the other equilibrium statistics that can be precalculated using unperturbed information. The additional computational expense for solving the scalar equation (4.11) is fairly low. The exponents in the scaling factors in (4.10) are consistent in dimension with the mean and variance corrections. The term multiplying dissipation scales with $E^{1/2}$ while the term multiplying noise scales with $E^{3/2}$ so that the additional corrections to higher statistics keep consistent in dimension with the third-order moment approximations in the real dynamics. This total energy correction introduce the global information into each spectral mode thus the nonlinear energy transfer structure can be better characterized in the imperfect model, while solving only one additional scalar equation (4.11) is the only additional cost in computation. Also the scaling factor from $E(t)$ introduces nonlinear global effects into the additional damping and noise corrections in each mode.

4.3. Summary of the reduced-order algorithm

Generally we will test two different strategies in designing the imperfect model parameters:

- *Gaussian closure model 1 (GC1)*: using constant additional parameters $(d_{M,\mathbf{k}}, \omega_{M,\mathbf{k}}, \sigma_{M,\mathbf{k}})$ directly from unperturbed equilibrium (4.6) and (4.7);
- *Gaussian closure model 2 (GC2)*: taking the parameters as in GC1 and further scaling them with proper statistical energy through (4.9) and (4.10).

The GC1 model is the most direct and possibly simplest approach for the corrections in replacement of the high-order interaction terms. However with large numbers of unresolved modes, the constant corrections become insufficient to capture the sensitive model responses with accuracy. As a further improvement, GC2 with the scaling factor can significantly improve the imperfect model sensitivity using the total statistical energy amplitudes. Also we compare GC1 and GC2 model together to illustrate the improvement through the total statistical energy calibration. We summarize the algorithm for the low-order statistical closure methods as the following algorithm.

Algorithm 4. *(Low-order statistical closure methods for barotropic system with topography)*

Choose the low-dimensional subspace $\mathbb{R}^M$ with orthonormal basis $\{\mathbf{e}_\mathbf{k}\}_{|\mathbf{k}|=-M}^{M}$. Set up statistical dynamical equations (4.4) for the first-order mean, $\left(\bar{U}, \bar{\psi}_\mathbf{k}\right)$, and (4.5) for the second-order covariances, $\left(r_U, c_{U\psi,\mathbf{k}}, r_{\psi,\mathbf{k}}\right)$, in the resolved subspace $\mathbb{R}^M$ for $1 \le |\mathbf{k}| \le M$, as well as the statistical energy or enstrophy equation (3.10) to get the total energy/enstrophy E in the system. The modeling process can be decomposed into two separate steps:

- *Calibration step:*
  - *Get the true linear response operator from the invariant measure with exact formulas (3.8), and calculate the imperfect model predicted linear response operator from proper estimation strategies (say, kicked response method);*
  - *Determine the imperfect model parameter values, $(d_{M,\mathbf{k}}, \omega_{M,\mathbf{k}}, \sigma_{M,\mathbf{k}})$, through the closure schemes GC1 or GC2; tune the additional free parameters through minimizing the information distance (4.8) between linear response operators;*
- *Prediction step:*
  - *Use the optimal tuned parameters achieved from the previous step to run the reduced-order model to predict first and second order statistics with any general specific external perturbations. Two approaches with increasing accuracy can be considered:*
    - *GC1 model: use constant additional damping and noise corrections;*
    - *GC2 model: scale the additional model parameters using the statistical energy from the total statistical energy equation (4.11).*

Note that in the calibration step in the algorithm, only the unperturbed statistics in equilibrium are required. Thus this offers the optimal model parameters that are ideally valid for all kinds of specific forcing perturbation forms [11]. With the help of the linear response operator we are able to find a unified way to tune the imperfect model parameters and avoid the exhausting and impractical process to tune the models each time with different kinds of perturbations.

5. Numerical tests about the reduced-order methods with the 57-mode model

In this section, we demonstrate the feasibility of the reduced-order methods developed in the previous sections for topographic barotropic equations. In the numerical simulations about the perfect system, the truncation $|\mathbf{k}|^2 \le N$ with $N = 17$ is utilized with 57 degrees of freedom, which forms a family of stringent paradigm models for topographic mean flow interaction. This model has the attractive features of the low-order truncated model being exactly like the three-dimensional Charney–DeVore model without dissipation and forcing [8], and consists of a well-defined mean climate state and topographic Rossby waves as well as an energy spectrum [34, 24, 25]. This perfect model has significant inhomogeneous statistical dynamics with blocked and unblocked regimes produced by turbulent backscatter from the Rossby waves. One representative feature in the flow field is the shift direction of the zonal mean flow from westward to eastward as the external forcing increases in amplitude. We will test the reduced-order methods' skill in predicting the most important large-scale statistics taking all these complex flow features in consideration.

5.1. A 57-mode simplified test model and its statistical properties

We apply the pseudo-spectral method to the topographic barotropic flow (2.1) and the fluctuation equations (2.7). For the truncated nonlinear advection term, $\mathcal{P}_N\left(\nabla^{\perp}\psi_N \cdot \nabla q_N\right)$, the 3/2-rule is applied to avoid aliasing error. In the perfect model, we choose wavenumber truncation at $N = 17$, that is, to consider a system in a 57-dimensional phase space. For the time integration, the standard 4th order Runge-Kutta methods are used with time step $\Delta t = 1 \times 10^{-3}$, which is small enough to capture all the small-scale dynamics. The random noise part is added through a standard Euler-Maruyama scheme. The time-series are recorded at every 10 time steps, that is, we sample the data at every 0.01 time unit. We integrate the system up to a long time with 1×10^7 time steps and the first 20000 steps are skipped in the calculation of model statistics. No additional hyperviscosity is needed in this small truncation case with only low wavenumbers included. In the reduced-order methods, we choose to use a three-dimensional resolved subspace, compared with the 57-dimensional full system

5.1.1. Simulations of the true barotropic system with layered topography

In the first test case, we begin with the topographic barotropic flow (2.1) using the simple layered topography with variation only in x-direction

$$h(x, y) \quad = \quad H(\cos x + \sin x). \tag{5.1}$$

(5.1) is the anisotropic one-mode topography which induces the interaction between the zonal topographic modes. This setting-up can be an analog to a long north-south ridge. Only the first lowest wavenumber is non-zero in the topography, thus the major interaction is between the large-scale mean flow, U, and the first topographic Rossby mode, $\mathbf{k} = (1, 0)$. The use of a single topographic Rossby mode here in the model is to provide a clean test set for statistical model reduction. All of the transfer of fluctuations from the other unresolved modes to the mean flow occurs through this single Rossby mode from the topographic stress. Different topographic strengths $H = \sqrt{2}/4, 3\sqrt{2}/4, 5\sqrt{2}/4$ have been tested in [24, 25] in order to exhibit a range of behaviours for the correlation functions. Typically, we check two cases with different damping and topographic strength as follows

- *weak coupling and strong damping rate* $H = 3\sqrt{2}/4, d = 0.5$: in this case, larger damping rate is applied to both small and large scale variables and the topographic stress is weaker. The system is mixing faster with weaker interaction between the small and large scale modes;
- *strong coupling and weak damping rate* $H = 5\sqrt{2}/4, d = 0.1$: in this case, smaller damping rate is applied to both small and large scale variables and the topographic stress is stronger. The system is coupled for longer time with stronger interactions between different modes due to the topographic stress.

In both test cases above, we use linear Ekman damping with $\lambda = 1$ in (3.6) so that the statistical energy equations as (4.11) is homogeneous and easy to solve for the reduced-order schemes. The amplitude of the random noise σ is set up according to the damping rate d so that the equilibrium energy level is $\sigma_{\text{eq}} = 1$ according to (3.8). In the unperturbed case, no deterministic external forcing is added in both large and small scales to the system, $\delta\hat{F}_{\mathbf{k}} = 0, \delta F_0 = 0$. In the perturbed case, forcing perturbations will be added to both large-scale mean flow $\delta F_0 = \delta F$ and the topographic Rossby mode $\delta\hat{F}_{(1,0)} = \delta F/3$ (the scale factor $\frac{1}{3}$ is added in small-scale forcing to make sure a balanced perturbation in both small and large scales) in a wide range $\delta F \in [-1.5, 1.5]$. In the 57-mode model, it is found that the steady state is insensitive to the different choices of initial values. The large and small scale initial condition is taken from the invariant measure (3.8) with a random perturbation consistent with the variances. The model parameters are listed in Table 1. The mean flow jet $\bar{U}$ changes direction as the external perturbation amplitude δF increases, switching from a weak westward flow ($\bar{U} < 0$) to an eastward flow ($\bar{U} > 0$) with a fairly abrupt transition in strength of the jet as illustrated in Figure 5.8.

In the first place, we check the true unperturbed dynamics with the statistical theory in Section 3. In Table 2, we compare the steady state statistics in the first spectral mode, $\psi_{(1,0)}$, and the large-scale mean flow, U. In the steady state statistical mean, the first topographic Rossby mode, $\psi_{(1,0)}$, is dominant, following the theoretical estimate, $\bar{\psi}_{\mathbf{k}} = \hat{h}_{\mathbf{k}}/\left(\mu + |\mathbf{k}|^2\right)$. The mean flow has a weakly west-moving jet $\bar{U} = -0.5$ in the unperturbed state. In the variances, it can be observed that more meridional modes become active in fluctuation containing larger energy in variance due

one-mode topography		β	μ	H	d	σ^2_{eq}	λ	Δt	δF
$H(\cos x + \sin x)$	weak coupling	1	2	$3\sqrt{2}/4$	0.5	1	1	1×10^{-3}	$[-1.5, 1.5]$
	strong coupling	1	2	$5\sqrt{2}/4$	0.1	1	1	1×10^{-3}	$[-1.5, 1.5]$

Table 1: Model parameters for the 57-mode model used in the numerical tests. Two typical cases with weak coupling, $d = 0.5, H = 3\sqrt{2}/4$, and strong coupling, $d = 0.1, H = 5\sqrt{2}/4$ are tested. δF is the perturbation amplitudes to the large-scale mean flow U and first topographic Rossby mode, $\mathbf{k} = (1, 0)$.

		$\bar{U}$	$\overline{U'^2}$	$\bar{\omega}_{(1,0)}$	$\overline{\lvert\omega'\rvert^2}_{(1,0)}$	$\overline{\lvert\omega'\rvert^2}_{(0,1)}$	$\overline{\lvert\omega'\rvert^2}_{(1,1)}$	$\overline{U'\omega'}_{(1,0)}$
weak	theory	-0.5	0.5	0.1768-0.1768i	0.3333	0.3333	0.1250	0
	numerics	-0.5228	0.5080	0.1764-0.1799i	0.3353	0.3350	0.1238	(2.5+1.8i) $\times 10^{-3}$
strong	theory	-0.5	0.5	0.2946-0.2946i	0.3333	0.3333	0.1250	0
	numerics	-0.4958	0.4953	0.2961-0.2955i	0.3366	0.3327	0.1246	(-4.0+4.0i)$\times 10^{-3}$

Table 2: Unperturbed equilibrium statistics of the 57-mode model in weak coupling case $d = 0.5, H = 3\sqrt{2}/4$ in upper part, and strong coupling case $d = 0.1, H = 5\sqrt{2}/4$ in lower part. The theoretical prediction from the Gaussian invariant measure (3.8) is compared with the results from direct numerical simulations in model (4.1). The first part is the mean and variance in the large-scale mean flow U, the second part is the mean and variances in the leading Fourier modes, and the last part shows the correlation between the small and large scale covariances. It can be seen that in this unperturbed case, the system reaches the Gaussian invariant measure with zero correlation between small and large scale variables.

to the nonlinear interactions between modes. Especially, the first meridional mode, $\psi_{(0,1)}$, becomes quite energetic with large variance, and the spectra appear to be radial symmetric as expected.

For more details about the 57-mode model statistics, Figure 5.1 plots the snapshots of the stream function ψ, the time evolution of the mean flow U, as well as the ratio of energy in the mean flow to display the interactions between the small and large scale variables. Two regimes with distinct blocked and unblocked structures in stream function can be observed in the snapshots and time-series. The flow stream function exchanges between two states in that one has large zonal velocity flow (unblocked regime), and one has quite small zonal flow but strong meridional transport (blocked). As the ratio of energy in the mean flow U becomes large, larger fluctuations can be observed in the time-series of the mean flow, showing strong energy transfers between the small and large scale variables. This is marked as the blocked regime due to the strong meridional flow $v = \partial_x \psi$ through the topographic stress $\oint hv$; while when the ratio of mean flow energy becomes small, the mean flow amplitudes also change in much smaller fluctuations, showing the unblocked regime with weaker energy transfer and strong zonal flow. In the following parts of the figure we compare the autocorrelation functions and pdfs of the most energetic modes. It can be observed that both the small and large scale modes have Gaussian marginal distributions consistent with the invariant measure predicted from the theory in (3.8). Despite the Gaussian pdfs the 57-mode paradigm model displays the physical reasonable metastable regime transitions between the blocked and unblocked zonal flows [34]. More discussions about the stability analysis due to topographic stress can be found in Chapter 5 of [4] and [27].

5.1.2. Linear response theory and FDT predictions

As discussed in the Section 3.1, FDT can offer first-order linear approximations in response to various external forcing perturbations. Here we check the skill and accuracy of FDT in the 57-mode model as a forcing perturbation, $(\delta F_0, \delta F_1)$, is added in both small and large scale variables. As described before, we only perturb the large-scale flow, $\delta F_0 = \delta F$, and the first Rossby topographic mode with wavenumber $\mathbf{k} = (1, 0)$, $\delta F_1 = \frac{1}{3}\delta F$ in the range $[-1.5, 1.5]$. The explicit form of the Gaussian invariant measure in the barotropic flow (4.1) offers the convenience to calculate the exact linear response operator and achieve first order predictions of the responses through FDT. The linear response operators, $\mathcal{R}_A$, corresponding to the first two moments using the exact invariant measure and formulas have already been derived in Appendix B in explicit formulation. Thus the leading order prediction from FDT in linear theory can be calculated directly through the formula (3.3) in response to external perturbations, δF.

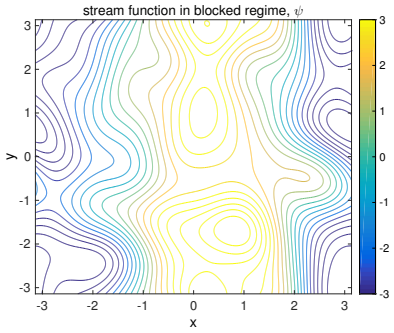

(a) stream function ψ (blocked regime)

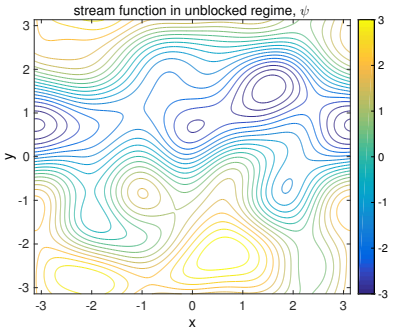

(b) stream function ψ (unblocked regime)

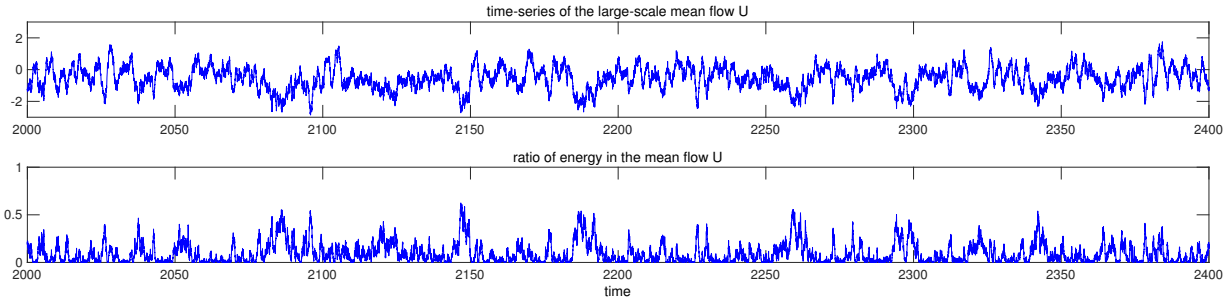

(c) time-series of mean flow U (weak coupling)

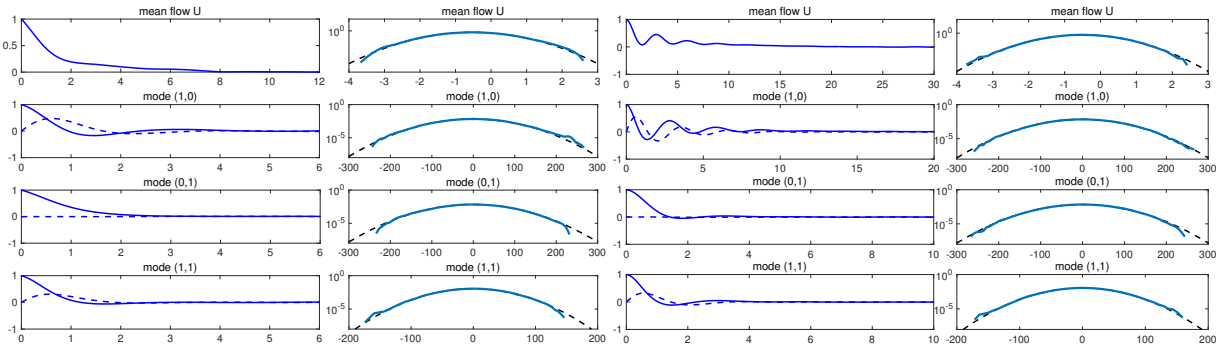

(d) weak coupling

(e) strong coupling

Figure 5.1: The unperturbed 57-model model in weak coupling case $d = 0.5, H = 3\sqrt{2}/4$ and strong coupling case $d = 0.1, H = 5\sqrt{2}/4$. The first row is the snapshots of the stream functions ψ in both blocked and unblocked regimes. The next two rows plot the time-series of the large-scale mean flow U and the ratio of energy in the mean flow. Autocorrelation functions (imaginary part in dashed lines) and probability distribution functions (in logarithmic coordinate) with one-mode topography in the most energetic modes in the 57-mode model are shown in the following parts in both cases. In the pdfs, Gaussian distributions with variances from theoretic prediction are also shown in dashed black lines.

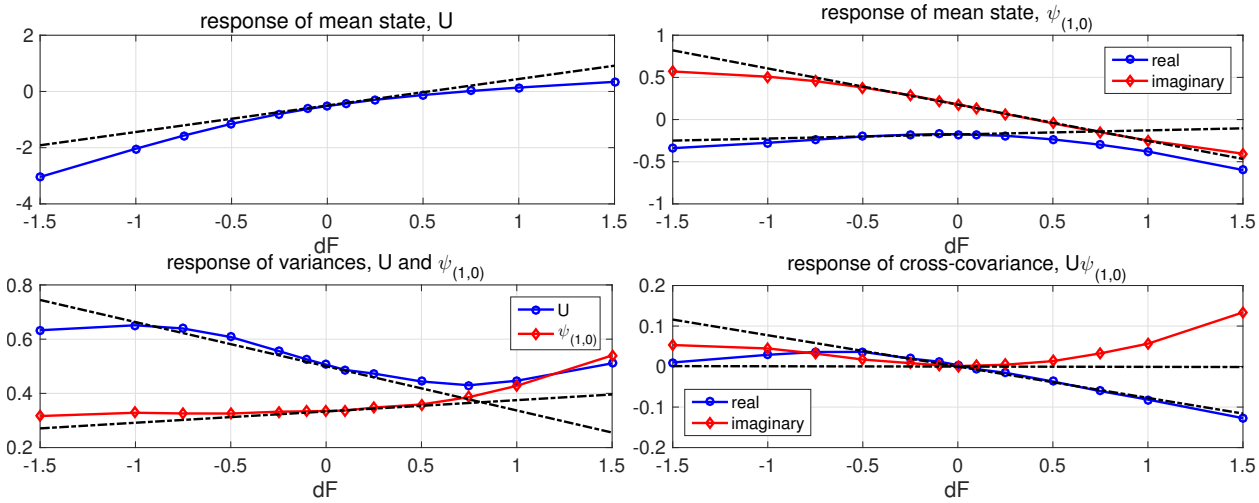

Figure 5.2: Nonlinear responses in the first and second moments in the 57-mode model in weak coupling case $d = 0.5, H = 3\sqrt{2}/4$ with perturbations in both small and large scale forcing terms, $\delta F \in [-1.5, 1.5]$. The linear predictions from FDT using the exact linear response operator from invariant measure is illustrated by black dotted-dashed lines.

The nonlinear model responses in first and second order moments about the large-scale mean flow U and the leading topographic Rossby mode $\psi_{(1,0)}$ with the prescribed forcing perturbation together with the FDT predictions are illustrated in Figure 5.2 for the weakly coupled regime. The perfect model responses to perturbations appear highly nonlinear in both mean and covariances with changing amplitude along positive and negative perturbations δF even in this weak coupling case. On the other hand, the FDT predictions are always linear and tangent to the true curve at $\delta F = 0$. With small perturbation amplitude, the FDT results can capture the response values with relative accuracy, whereas as the perturbation amplitude δF increases the strong nonlinearity ends up with large error in linear FDT predictions even though the exact linear response operator $\mathcal{R}_A$ is used. Note also the cross-covariance between the large-scale mean and small-scale modes, $\overline{U'\psi'}_{(1,0)}$, stays zero as no perturbation $\delta F = 0$ is applied, whereas large non-zero deviation in the cross-covariance appears with non-zero perturbation showing nonlinear interactions between the large and small scale modes. Further in the strong coupling case with weaker damping and larger topographic stress, the modes are correlated for a longer time. This implies stronger interactions between the large-scale mean and the small-scale topographic modes. Therefore stronger nonlinear responses are expected.

Still notice that in calculating the responses in FDT, we only use the integrated values of the linear response operator, $R_A = \int \mathcal{R}_A$. Thus many useful information is ignored during this process. So by fitting these exact linear response operators under the information metric (4.8) in the reduced-order methods, improvement in the prediction skill in responses can be expected with the help of low-order models in the next section.

5.2. Reduced-order methods for barotropic system with layered topography

Here we test the statistical closure methods' ability in capturing these responses to perturbations. The reduced-order statistical closure models are proposed to capture the most important statistics in the system. The crucial first and second order moments are calculated in the reduced-order models with only 3 resolved modes (that is, the mean flow U together with the real and imaginary part of the topographic mode, $\psi_{(1,0)}$) comparing with the 57-dimensional full system. The methods are displayed in the model calibration training phase for optimal parameters, and model forecast phase for predicting principal responses.

5.2.1. Tuning imperfect model parameters in the training phase

In the reduced-order models (4.4) and (4.5), we have two important free parameters $(d_{M,0}, d_{M,k})$ as the additional damping in large and (resolved) small scales to determine for the optimal value. Generally $d_{M,k}$ is the most important one controlling the errors in the small-scale modes, where most of the errors come from due to the imperfect characterization of the triad interactions. In the training phase the optimal model parameters are selected through

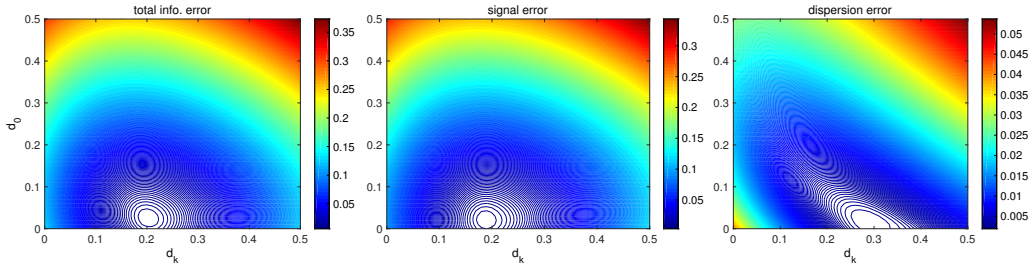

(a) Errors with changing $d_{M,k}, d_{M,0}$

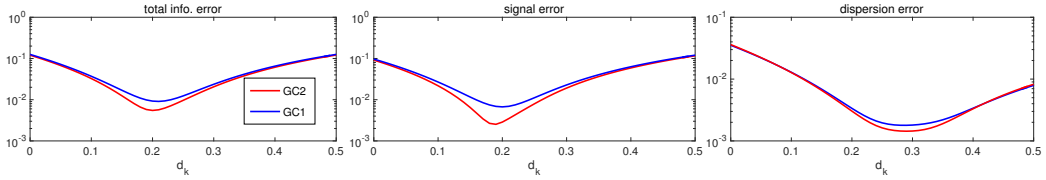

(b) Compare the error in GC1 and GC2

Figure 5.3: Tuning imperfect model parameters in the weakly coupling case $d = 0.5, H = 3\sqrt{2}/4$. The first row compares the total information error together with the errors in signal and dispersion part with changing $d_{M,k}$ and $d_{M,0}$ using GC2 model. The second row compares the errors between imperfect model GC1 and GC2 with changing $d_{M,k}$. The optimal value with minimum error is reached at $d_{M,0} = 0.03$, $d_{M,k} = 0.2$, $\omega_{M,k} = -0.05$.

minimizing the information error (4.8) among a domain of possible values. Figure 5.3 shows the tuning results for imperfect model parameters in the weakly coupling case. The first row compares the total information error together with the errors in signal (second row in (4.8)) and dispersion (third row in (4.8)) part with changing $d_{M,k}$ and $d_{M,0}$ using GC2 model. The second row compares the errors between imperfect model GC1 and GC2 with changing $d_{M,k}$ and optimal $d_{M,0}$. It appears that only small correction $d_{M,0}$ is need for the large-scale correction. And small difference appears in the GC1 and GC2 model here (still the necessity of using GC2 with additional energy correction will be shown in the prediction phase next). Overall, there exists a wide regime of parameter values where the information distance stays in low errors, reflecting the robustness of the methods.

In Figure 5.4 and 5.5 we compare the linear response operators $\mathcal{R}_A(t)$ for the mean and variances using the optimal parameters in the imperfect model with the truth. Both results of weakly coupling and strongly coupling case are shown. It can be seen that the mean and variances can be both recovered with high accuracy in the weakly coupling case. From the information error, the errors in the beginning transient regime is as small as the following fluctuation errors due to the noises in the true data. In the strongly coupling case, the fitting through imperfect models is tougher considering the stronger interactions through the topographic stress. Still good agreement can be achieved capturing the oscillatory structure in both mean and variance linear response. Besides, GC1 and GC2 model offer similar approximations in this training phase.

5.2.2. Predicting model responses to external perturbations

In this part, we check the prediction skill of the low-dimensional imperfect models in capturing responses to various external perturbations in different regimes. Only a 3-dimensional reduced-order subspace of $\{U, \Re\mathrm{e}\psi_{(1,0)}, \Im\mathrm{m}\psi_{(1,0)}\}$ is resolved compared with the 57-dimensional true system (with covariance matrix of dimensionality $57^2 \sim 3200$). Especially in this case with independent Gaussian invariant measure (3.8) in unperturbed system, the climate information can offer no correction for the perturbed responses in cross-covariances (say, $\overline{U'\psi'_{\mathbf{k}}}$ and $\overline{\psi'_{\mathbf{k}}\psi'^{*}_{\mathbf{l}}}$), whereas these covariances become non-zero and crucial even when small perturbations are applied as already shown in Figure 5.2. This adds additional difficulty in achieving accurate prediction results especially when larger perturbations are applied. Of special interest here, we focus on the models' skill in capturing the mean and variances in the mean flow U and first topographic Rossby wave $\psi_{(1,0)} = -\omega_{(1,0)}$. Due to the nonlinear energy transfer between the small and large scales and the frequent transition of blocked and unblocked regime, nontrivial nonlinear complicated responses are generated in both the mean and covariances. Observing the responses in the large-scale mean jet U, the mean jet

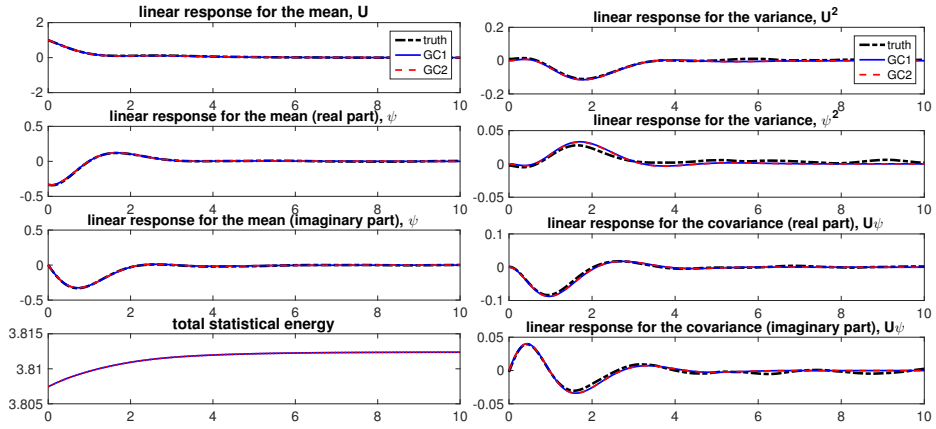

(a) mean state (b) variance

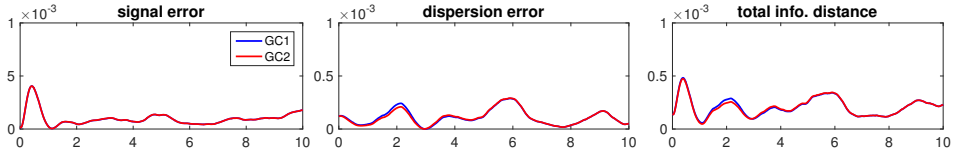

(c) information error

Figure 5.4: Linear response operators, $\mathcal{R}_A(t)$, for the first two moments with optimal parameters in the weakly coupling case $d = 0.5, H = 3\sqrt{2}/4$. The corresponding information error as well as the errors in signal and dispersion parts is compared in the last row. The results for GC1 model (blue) almost overlap with GC2 model results (red) together with the truth (black). And note that especially for the dispersion part of the error, the errors in the beginning transient regime is almost as small as the fluctuations in the final steady state.

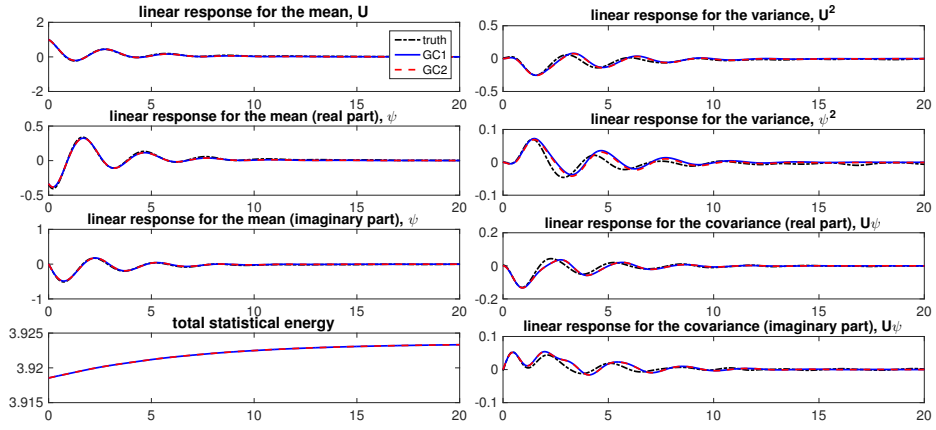

(a) mean state (b) variance

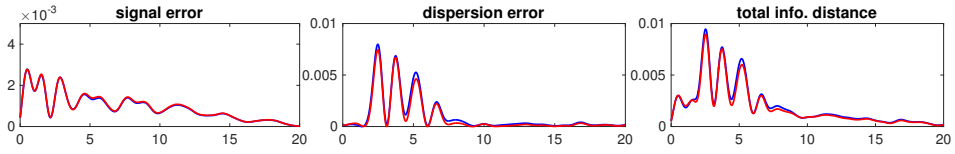

(c) information error

Figure 5.5: Linear response operators, $\mathcal{R}_A(t)$, for the first two moments with optimal parameters in the strongly coupling case $d = 0.1, H = 5\sqrt{2}/4$. Imperfect model results GC1 and GC2 almost overlap with the truth especial in the mean responses. The optimal value with minimum error is reached at $d_{M,k} = 0.22$, $d_{M,0} = 0.04$, $\omega_{M,k} = -0.05$.

strength $\bar{U}$ switches direction from a westward flow to eastward moving like nature as the perturbation δF increases in amplitude in both cases.

In Figure 5.6, prediction skills of imperfect closure models GC1 (blue) and GC2 (red) compared with the truth (black) in response to a wide range of external perturbation amplitudes in the forcing δF in the weakly coupling case $d = 0.5, H = 3\sqrt{2}/4$ are compared. The responses in the mean and variance of the large-scale mean flow U and first topographic mode $\psi_{(1,0)}$ as well as their cross-covariance between small and large scales $\overline{U'\psi'}_{(1,0)}$ are plotted. The total statistical energy E through the energy dynamics is also compared in the last row. GC1 and GC2 model display similar skills when perturbations are small, while the errors in GC1 become larger as the perturbation amplitude increases. In general these two models both offer accurate overall predictions for the nonlinear responses in both first and second order moments in this weak coupling regime. In Figure 5.7, we check the more difficult case with strong coupling between modes, $d = 0.1, H = 5\sqrt{2}/4$. Strong nonlinear responses appear in both mean and covariances in this test regime as perturbations are applied. GC1 and GC2 model offer similar accurate recoveries for the responses in the mean estimation with minor difference, while larger errors appear in GC1 for the response predictions in the second order moments. This is due to the stronger higher order statistics that are not resolved in the reduced-order closure models and GC1 lacks the detailed correction calibration from the statistical energy equation. Still in the results corresponding to various perturbations, the imperfect model GC2 predictions are accurate for most of the regimes. The effectiveness of the total statistical energy correction can be displayed by comparing GC1 and GC2 results in the variance predictions. Note that when the forcing perturbation becomes extremely large in the positive values, $\delta F \geq 1$, a bifurcation takes place in the system. Thus the state variables shift to another fixed point, so that the reduced-methods lose the ability to capture the responses. Still we suspect that the reduced-order model skill can be resumed with measurement in the new shifted state, but we leave this to further investigation in the future.

In testing the perturbed model responses, one important observation is that the value of the large-scale mean flow U will take an abrupt transition to the other state as we slowly increase the amplitude forcing perturbations δF. The change of state (or bifurcation) may introduce further difficulties in the applications of reduced-order methods, because we can only use the statistical steady state information of the unperturbed state and after the bifurcation the statistics in the perturbed system may become entirely different, thus leading to failure of the statistical closure methods. As shown in Figure 5.8 for the snapshots of stream functions Ψ and time-series of the mean flow U, the flow field is shifting between the west going and east going jets as the system evolves in time with perturbation amplitude $\delta F = 0.75$ as an example; between the perturbation values δF from 0.75 to 1, a bifurcation takes place shifting large-scale mean flow to eastward with a strong positive mean state. Beyond the bifurcation value it becomes difficult for predicting the model responses by only relying on the unperturbed steady state statistics.

5.3. Reduced-order methods for fluctuation equations of the barotropic flow

In the above tests for topographic barotropic system (2.1), we always assume the desirable situation with a Gaussian invariant measure in the unperturbed equilibrium state with zero deterministic forcing. However in many realistic scenarios, non-Gaussian statistics might be even inherent in the unperturbed statistics in equilibrium. Here we study this situation using the fluctuation equations (2.7) with a non-zero deterministic forcing in the 'climate' driving the unperturbed state away from Gaussian statistics.

5.3.1. Testing regime for the fluctuation equations with non-Gaussian climate

The fluctuation equations (2.7) focus on the state variable deviations $\left(\tilde{U}, \tilde{\psi}\right)$ from the original unperturbed equilibrium mean state $\left(\bar{U}_{\text{eq}}, \bar{\psi}_{\text{eq}}\right)$. It is worthwhile to check the model responses in the fluctuation equations when constant deterministic forcing $\mathcal{F}$ is always applied in the background. We choose to test the models in the representative strong coupling case with parameters the same as the case in Table 1, whereas we would like to also introduce the effects from different kinds of damping forms as i) the original linear Ekman damping, $-d\omega$; and ii) the combined damping form in consistent with the pseudo-energy, $-d(\omega - \mu\psi)$ from (3.6). And instead of the layered topography as in the previous case, we propose more complexity in the topography by superimposing small-scale disturbances on top of the large-scale basic topographic mode

$$h = H(\cos x + \sin x) + H' \sum_{1<|\mathbf{k}|\leq\Gamma} \frac{e^{i(\mathbf{k}\cdot\mathbf{x}+\theta_0)}}{|\mathbf{k}|^p} + c.c. \tag{5.2}$$

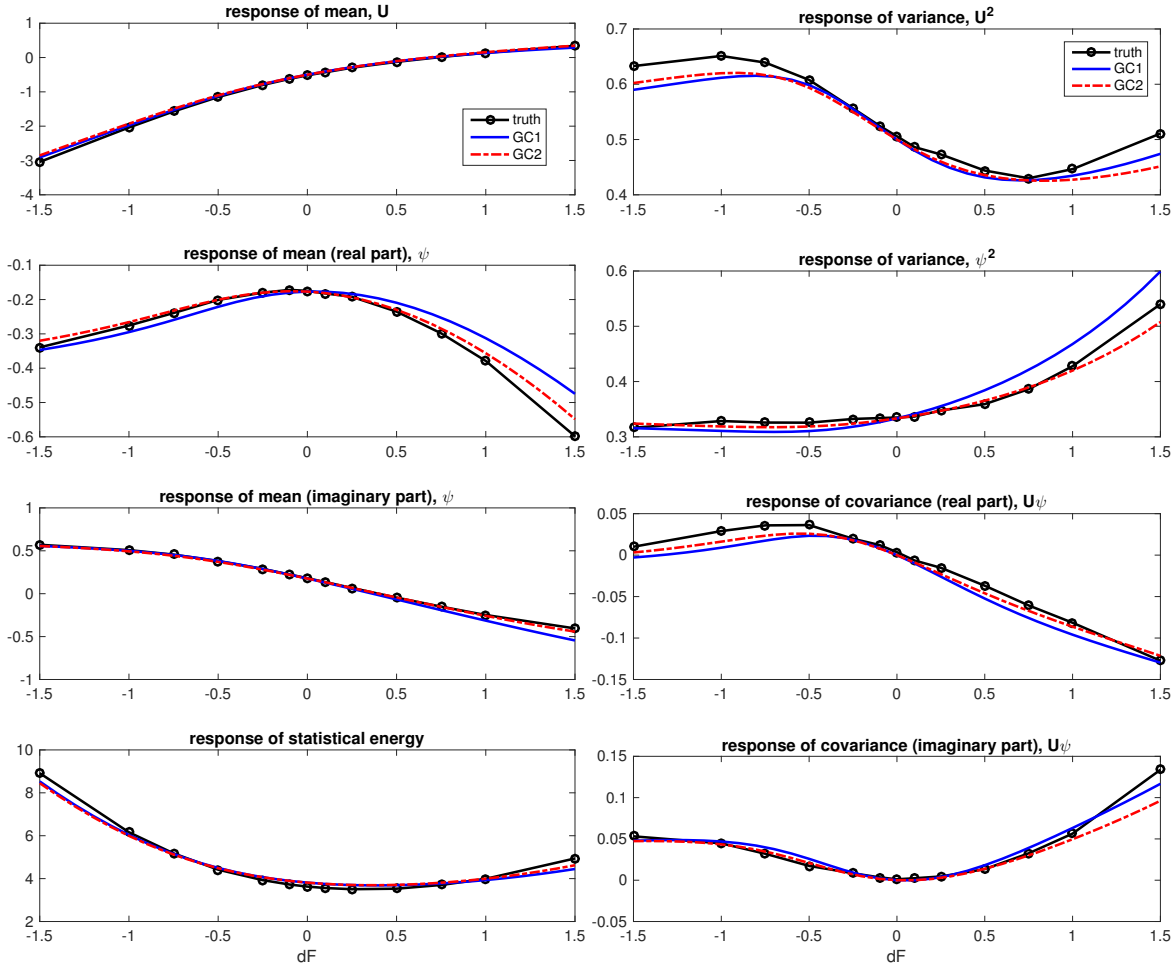

(a) response of mean

(b) response of variances

Figure 5.6: Prediction skill of imperfect closure models GC1 (blue) and GC2 (dotted-dashed red) compared with the truth (black with circles) in response to various external perturbation amplitudes in the forcing range $\delta F \in [-1.5, 1.5]$ in the weakly coupling case $d = 0.5, H = 3\sqrt{2}/4$. The responses in the mean and variances of the large-scale mean flow U and first topographic mode $\psi_{(1,0)}$ as well as their cross-covariance $\overline{U'\psi'}_{(1,0)}$ are compared. GC1 and GC2 models display similar skills with small perturbations, and the errors for GC1 becomes larger as the perturbation amplitude increases. In general these two models both offer accurate overall predictions.

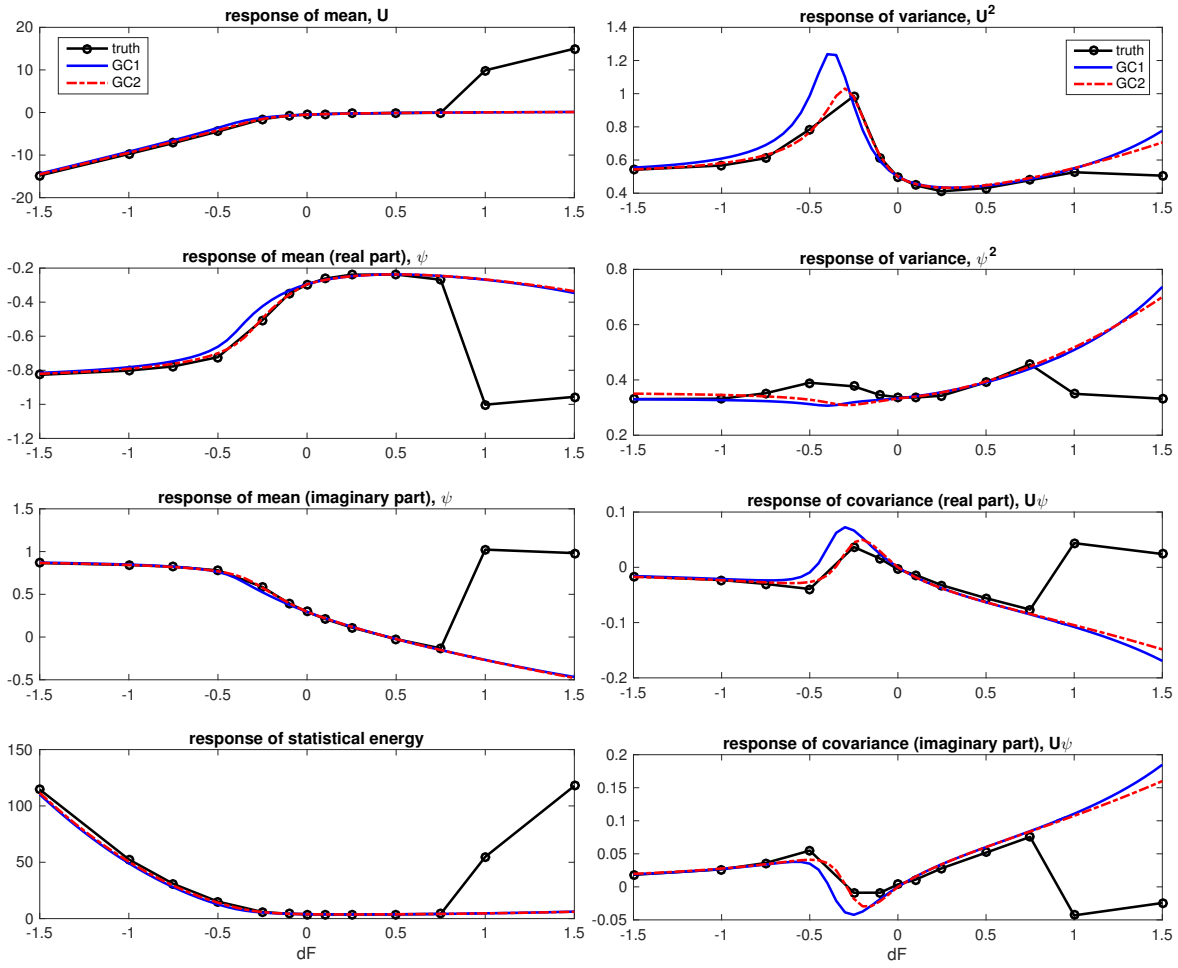

(a) response of mean

(b) response of variances

Figure 5.7: Prediction skill of imperfect closure models GC1 (blue) and GC2 (dotted-dahsed red) compared with the truth (black with circles) in response to various external perturbation amplitudes in the forcing range $\delta F \in [-1.5, 1.5]$ in the strongly coupling case $d = 0.1, H = 5\sqrt{2}/4$. The responses in the mean and variances of the large-scale mean flow U and first topographic mode $\psi_{(1,0)}$ as well as their cross-covariance $\overline{U'\psi'}_{(1,0)}$ are compared. In this strongly coupling case, the nonlinear interactions between modes become stronger, making it a more difficult regime to capture the responses with accuracy. Bifurcation to another state takes place when extremely large perturbation $\delta F \geq 1$ is added. After the bifurcation, the closure model loses the skill in capture the right responses.

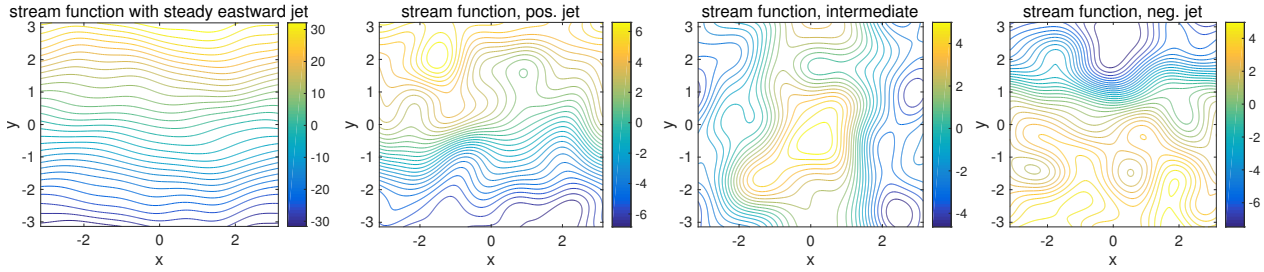

(a) snapshots for $\delta F = 1$

(b) snapshots of total stream functions $\Psi = -Uy + \psi$ for $\delta F = 0.75$

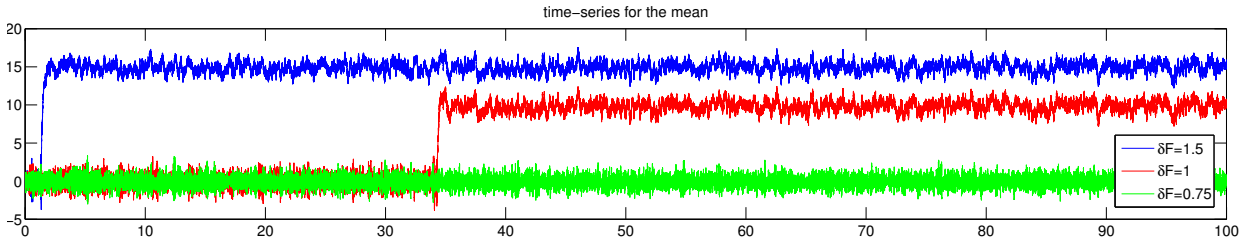

(c) time-series of zonal mean flow U

Figure 5.8: Snapshots of total stream functions $\Psi = -Uy + \psi$ for $\delta F = 0.75, 1$, and time series of the large-scale mean flow when large forcing perturbations $\delta F \geq 0.75$ are applied. The original fixed point becomes unstable and the flow transfers to another stable fixed point away from the original value as the perturbation amplitude increases.

Above θ_0 is the phase shift, whereas, p controls the smoothness of the small-scale features. $c.c.$ represents the complex conjugate part to make sure the variables to be real in physical domain. In following tests we always take the parameter values, $\theta_0 = \frac{\pi}{4}, p = 2$, for the small-scale topographic disturbances. The topographic strength is chosen relatively strong as $H = 5\sqrt{2}/4$, where more non-Gaussian structures can be generated. Note that symmetry is broken in this topography setting-up since the meridional modes is zero, $\hat{h}_{(0,\pm 1)} = 0$. The deterministic forcing terms in the unperturbed case are added in the *generalized Kolmogorov forcing* form as

$$\mathcal{F}(\mathbf{x}, t) = \sum_{|\mathbf{k}|=1} \hat{F}_{\mathbf{k}}(t)\, e^{i\mathbf{k}\cdot\mathbf{x}} + c.c. \tag{5.3}$$

Always in our following numerical tests, the deterministic forcing is exerted on the largest scale modes, $|\mathbf{k}| = 1$ (that is, for Fourier modes, $\hat{F}_{(\pm 1,0)}$ and $\hat{F}_{(0,\pm 1)}$), to simulate the effects such as surface wind driving or radiative heating. Besides, a constant forcing, $\mathcal{F}_0$, is also asserted on the large-scale mean flow U. The deterministic forcing strength in the lowest wavenumber is taken as $\hat{F}_1 = 2$.

With the above described forcing and topography, the major (nonlinear) interactions take place between the large-scale mean flow, U, and the forced topographic Rossby modes, $(\pm 1, 0)$ and $(0, \pm 1)$. Note that the nonlinear transfer of energy between modes $(\pm 1, 0)$ and $(0, \pm 1)$ are always through the intermediate mode $(1, 1)$ (which will not be resolved in our reduced models, that makes the model reduction methods even more challenging). Table 3 first shows the equilibrium statistics in the unperturbed case with constant forcing. The equilibrium states for the mean and covariance are altered due to different damping operators. Stronger covariances between $U, \omega_{(1,0)}, \omega_{(0,1)}$ can be observed in both cases. Snapshots and statistics are illustrated in Figure 5.9. Inhomogeneous structure can be observed in the snapshots, and dominant modes with $|\mathbf{k}| = 1$ can be observed in the mean stream functions. Autocorrelation functions oscillate for a long time with large decorrelation time. Strong sub-Gaussian marginal distributions appear in the unperturbed fluctuation modes. This is due to the constant deterministic forcing applied in the background.

5.3.2. Imperfect model responses to perturbations in the fluctuation equations

In these testing cases for the fluctuation equations, we also focus on the application of the reduced-order models to be utilized to approximate the geophysical flow responses in statistical mean and variance. The two typical damping

	$\bar{U}$	$\bar{\omega}_{(1,0)}$	$\bar{\omega}_{(0,1)}$	$\overline{U'\omega'}_{(1,0)}$	$\overline{U'\omega'}_{(0,1)}$	$\overline{U'\omega'}_{(1,1)}$
linear damping	20.4813	0.64-0.67i	1.57+0.21i	-0.21+0.20i	0.0079+0.0084i	0.027-0.048i
combined damping	21.4550	0.62-0.71i	3.75+0.25i	-0.31+0.30i	0.019+0.0032i	0.034-0.067i
	$\overline{U'^2}$	$\overline{\lvert\omega'\rvert^2}_{(1,0)}$	$\overline{\lvert\omega'\rvert^2}_{(0,1)}$	$\overline{\omega'_{(1,0)}\omega'^*_{(-1,0)}}$	$\overline{\omega'_{(2,0)}\omega'^*_{(-2,0)}}$	$\overline{\omega'_{(1,0)}\omega'^*_{(0,1)}}$
linear damping	0.5238	4.3512	3.4610	-0.0015-0.0033i	0.21+0.022i	0.022+0.058i
combined damping	0.5186	6.7885	3.9954	-0.0028-0.0053i	0.93-0.18i	0.035+0.11i

Table 3: Unperturbed equilibrium statistics of the fluctuation equations with damping and forcing (linear Ekman damping, $-d\omega$; and combined damping, $-d(\omega - \mu\psi)$). The parameters $\mu = 2, \sigma^2_{\text{eq}} = 1, \beta = 1, H = 5\sqrt{2}/4, d = 0.1$ are used in the test. It can be seen that in this unperturbed case with non-zero deterministic forcing, some cross-covariances between different modes become important.

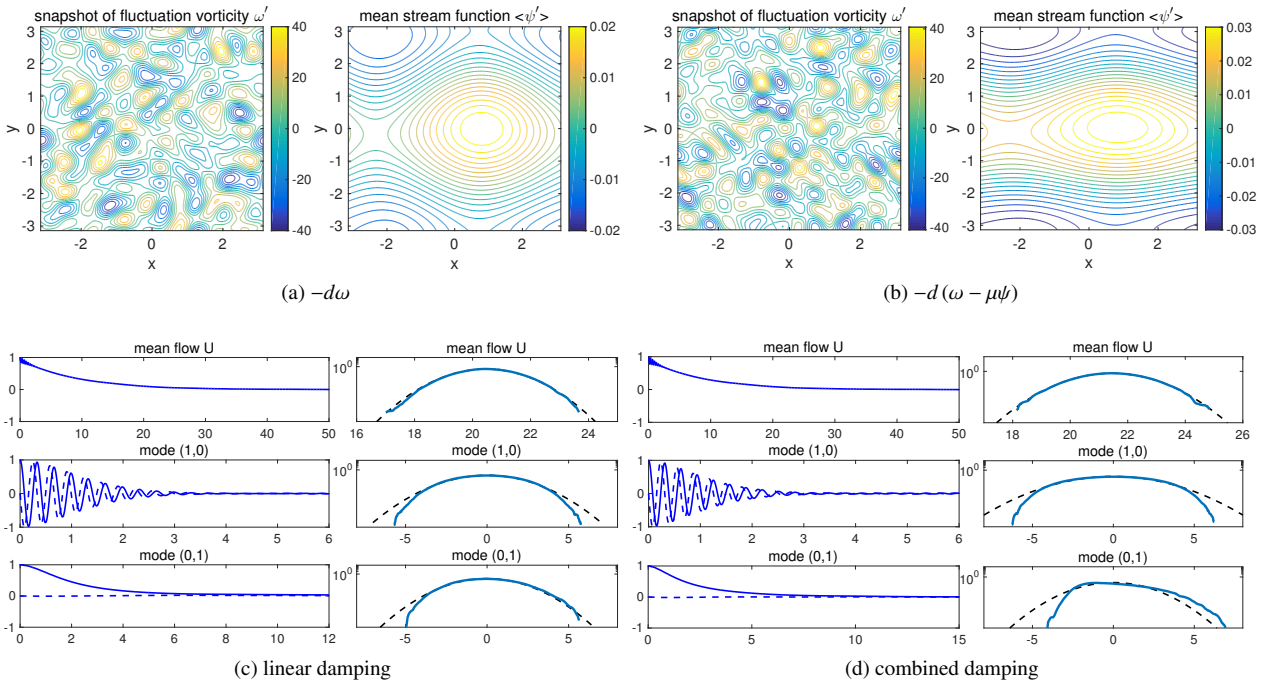

(a) $-d\omega$ (b) $-d(\omega - \mu\psi)$

(c) linear damping (d) combined damping

Figure 5.9: Statistics about the unperturbed fluctuation equations with linear Ekman damping, $-d\omega$ (left), and combined damping, $-d(\omega - \mu\psi)$ (right). Snapshots of the fluctuation vorticity ω and mean stream function $\bar{\psi}$ are compared in the first row. Autocorrelation functions (imaginary part in dashed lines) and probability distribution functions (in logarithmic coordinate) in the most energetic modes in the fluctuation model follow next. In the pdfs, we also compare with Gaussian distributions with the same variance in dashed black lines. Note that in this forced case, the autocorrelation functions oscillate for longer time thus the decorrelation time becomes much larger. In the forced modes, $(1, 0)$ and $(0, 1)$, the probability distributions are skewed with sub-Gaussian features.

terms with linear damping, $-d\omega$, and combined damping, $-d(\omega - \mu\psi)$, are both tested. Perturbations are added in the large-scale mean flow, δF_0, and the small-scale modes, $\delta F_{\mathbf{k}}$ with wavenumber $|\mathbf{k}| = 1$. The perturbation scales change in the range $\delta F \in [-1, 1]$ compared with the unperturbed forcing value $F = 2$ (that is, a 50% perturbation of the original unperturbed value). Especially with the strongest positive external perturbation, $\delta F = 1$, highly non-Gaussian structure could be induced through the strong nonlinear interactions between modes throughout the spectra. Also the small-scale disturbance in topography induces stronger topographic stress between the large-scale mean flow and small-scale fluctuation modes. Accordingly we choose a larger number of resolved modes in a 5 dimensional subspace spanned by U and $\omega_{(1,0)}, \omega_{(0,1)}$ in the reduced-order models which is still small compared with the total 57-dimensional phase space.

Following the same procedure as the development of reduced-order algorithms in Section 4.2, the optimal model parameters for the fluctuation equations should also be tuned in the first training stage for accurate imperfect model prediction skill. We neglect the detailed tuning results here and directly show the response forecasts in the prediction phase. In Figure 5.10, reduced-order model predictions with combined damping, $-d(\omega - \mu\psi)$, are compared. The true responses from the original model is shown in black lines, GC1 results are plotted in blue lines, while GC2 results are in dotted-red. Both model responses in the mean and covariances in both the large-scale mean flow U and the leading modes of ω are compared. For perturbations in the negative direction, the predictions are quite desirable with accurate estimation for both mean and second-order moments. As the perturbation goes to the positive direction, more non-Gaussian statistics will be introduced, and larger deviations in the imperfect model prediction from the truth appear. Strong nonlinearity through the third moments can be expected in these extreme large perturbation cases showing inherent barrier for the reduced methods. Comparing the results between GC1 and GC2 model, much larger errors will take place in the GC1 predictions in this situation. This is not surprising since no corrections from the total energy is used and only constant damping and noise are applied in this model. Overall, GC2 can offer good approximations in both mean and variance predictions. Especially note that the total statistical energy is captured well in both regimes, thus the scaling factor E using total energy structure can effectively improve the imperfect model sensitivity in GC2. Similar results can be observed in Figure 5.11 for linear damping, $-d\omega$. Again GC2 model maintains the skill in capturing responses in both mean and variances in both small and large scales under this 5-dimensional low-order model calculating only the first two moments compared with the 57-dimensional full system with strong non-Gaussian statistics.

6. Conclusions and Future work

We have investigated the statistical solutions of the barotropic equations for mean flow and small-scale interaction via topographic stress using statistical reduced-order closure models. Model consistency in equilibrium and sensitivity to external perturbations are both considered. It is known that imperfect models with statistical equilibrium fidelity still suffer inherent information barrier in model sensitivity to perturbations [15]. To improve model prediction skill for various responses to forcing perturbations, the low-dimensional reduced-order models follow the generic information-theoretic framework introduced in [11] measuring the information error in the linear response operators with only unperturbed equilibrium statistics used in a training phase before the prediction. The advantage is that the optimal model parameters, once achieved in the training phase, can be applied for the prediction of different kinds of specific perturbation forms in the external forcing. A general statistical theory for turbulent systems [31] is applied to the the one-layer barotropic model with specific damping and random forcing, where a Gaussian invariant measure is generated in the statistical steady state. Statistical theories concerning the linear response theory and the statistical energy dynamics are then discussed. These statistical theoretical results help the construction of the reduced-order methods and improve the imperfect model sensitivity using the total statistical energy structure. The feasibility of the reduced-order models is checked on both the topographic barotropic flow and the related fluctuation equations under a 57-mode paradigm model. Numerical solutions of the true system reveal prototype topographic blocked and unblocked patterns, and the zonal mean jet changes direction from westward to eastward as the external forcing perturbation is applied. In different dynamical regimes with strong nonlinear dynamics, the methods display high skill in capturing the nonlinear model responses in a wide range of external forcing perturbations, compared with the only first-order linear FDT predictions.

The systematic approach we develop in this paper can be extended to a number of important climate models directly such as two-layer models or barotropic flow on the sphere. As a direct generalization, the low-dimensional

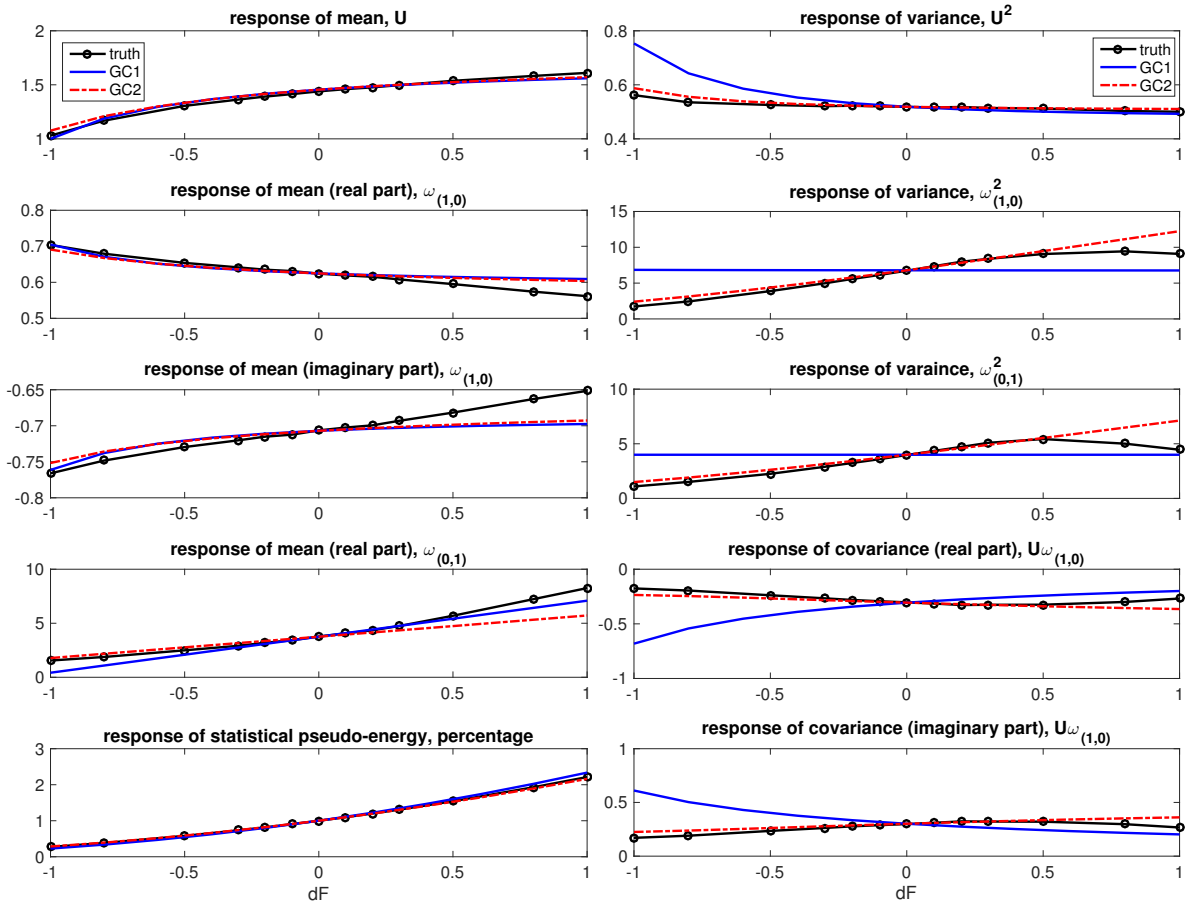

(a) responses in the mean

(b) responses in the variance

Figure 5.10: Reduced-order model predictions for the combined damping, $-d\,(\omega - \mu\psi)$. The true responses from the original model is shown in black line, GC1 results are plotted in blue lines, while GC2 results are in dotted-red. The left part shows the responses in the mean, and the right part shows the responses in second moments.

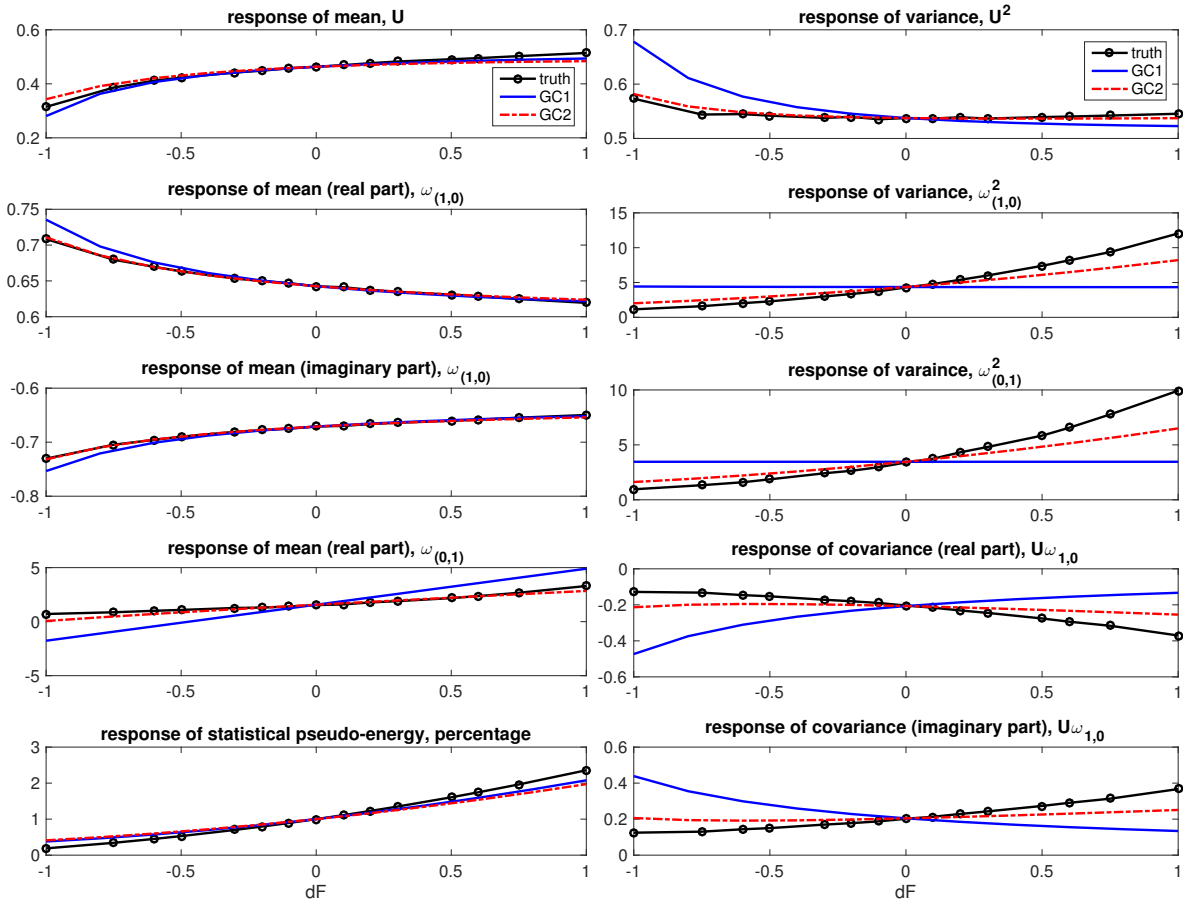

(a) responses in the mean

(b) responses in the variance

Figure 5.11: Reduced-order model predictions for the linear damping, $-d\omega$. The true responses from the original model is shown in black line, GC1 results are plotted in blue lines, while GC2 results are in dotted-red. The left part shows the responses in the mean, and the right part shows the responses in second moments.

reduced-order models can be used for predicting model sensitivity with other geometry (like flow on the sphere) and with more complicated vertical structure (like multi-layer models and even the Boussinesq equations). In these cases, baroclinic instability will take place and add larger uncertainty into the systems and stronger cascades of energy and enstrophy along the spectra can be expected. Besides, passive tracer advected by the geophysical turbulent flow also contains a number of attractive features and is worth investigating under this framework; reduced-order models are also required for capturing the passive tracer turbulence. The intermittent structure in the passive tracer field has been discussed in [35, 36]. It is worthwhile to pursue similar analysis and application of the reduced-order models about tracer advection in the geophysical flow.

Acknowledgment

This research of the Andrew Majda is partially supported by the Office of Naval Research through MURI N00014-16-1-2161 and DARPA through W911NF-15-1-0636. Di Qi is supported as a graduate research assistant on these grants.

Appendix A. The existence of Gaussian invariant measure in a general turbulent system

We offer more details about the general statistical theory in the abstract formulation about a family of general turbulent systems

$$\frac{d\mathbf{u}}{dt} = B(\mathbf{u},\mathbf{u}) + L\mathbf{u} - d\Lambda\mathbf{u} + \mathbf{F} + \Lambda^{1/2}\sigma\dot{\mathbf{W}}, \quad \mathbf{u} \in \mathbb{R}^N. \tag{A.1}$$

Nonlinearity is introduced through the quadratic form $B(\mathbf{u},\mathbf{u})$. The following general relations are required for the operators in (A.1):

$$\text{Skew Symmetry for } L, \qquad \mathbf{u}\cdot L\mathbf{u} = 0, \tag{A.2a}$$

$$\text{Energy Conservation}, \qquad \mathbf{u}\cdot B(\mathbf{u},\mathbf{u}) = 0, \tag{A.2b}$$

$$\text{Liouville Property}, \qquad \mathrm{div}_{\mathbf{u}}(B(\mathbf{u},\mathbf{u})) = 0, \tag{A.2c}$$

with the dot-product defined according to a proper metric from conserved 'energy', $\mathbf{u}\cdot\mathbf{v} \equiv \sum_j w_j u_j v_j$. The parameter Λ satisfies $\Lambda \geq 0$ as a fixed positive definite matrix, and $\Lambda^{1/2}$ is the square root according to the properly defined inner-product; $\sigma_{\mathrm{eq}}^2 = \frac{\sigma^2}{2d}$ defines the equilibrium energy level of the system. We offer the proof for Proposition 1 from the main text.

Proposition. *(Existence of Gaussian invariant measure) The turbulent system (A.1), associated with the structural properties in (A.2) and no deterministic forcing* $\mathbf{F} = \mathbf{0}$*, has a Gaussian invariant measure* p_{eq} *in statistical steady state; furthermore, the invariant measure has equipartition of energy in each component of* $\mathbf{u}$*,*

$$p_{\mathrm{eq}}(\mathbf{u}) = C^{-1}\exp\left(-\frac{1}{2}\sigma_{\mathrm{eq}}^{-2}\mathbf{u}\cdot\mathbf{u}\right), \tag{A.3}$$

with $\sigma_{\mathrm{eq}}^2 = \sigma^2/2d$ *defining the energy level.*

Proof. The Fokker-Planck Equation for the general system (A.1) with damping and random forcing, using the properties (A.2) in Section 3, is given by

$$\begin{aligned}\frac{dp}{dt} &= -\mathrm{div}_{\mathbf{u}}\left[(B(\mathbf{u},\mathbf{u}) + L\mathbf{u})\,p\right] + \mathrm{div}_{\mathbf{u}}(d\Lambda\mathbf{u}p) + \mathrm{div}_{\mathbf{u}}\left(\frac{\Lambda\sigma^2}{2}\nabla p\right)\\ &= -(B(\mathbf{u},\mathbf{u}) + L\mathbf{u})\cdot\nabla p + \mathrm{div}_{\mathbf{u}}\left(d\Lambda\mathbf{u}p + \frac{\Lambda\sigma^2}{2}\nabla p\right).\end{aligned}$$

The first equality uses the Liouville property of the quadratic operator B. The first part on the right hand side of the above equation vanishes, using the equilibrium measure $\nabla p_{\mathrm{eq}} = -\sigma_{\mathrm{eq}}^{-2}\mathbf{u}p_{\mathrm{eq}}$ together with the energy conservation of B and skew-symmetry of L.

For the second part of, insert p_{eq} inside and use the equilibrium energy level $\sigma_{\text{eq}}^2 = \sigma^2/2d$ we get

$$d\Lambda \mathbf{u} p_{\text{eq}} + \frac{\Lambda\sigma^2}{2}\nabla_{\mathbf{u}} p_{\text{eq}} = d\Lambda \mathbf{u} p_{\text{eq}} - \frac{\Lambda\sigma^2}{2}\sigma_{\text{eq}}^{-2}\mathbf{u} p_{\text{eq}} \equiv 0.$$

Therefore $p_{\text{eq}} = C^{-1}\exp\left(-\sigma_{\text{eq}}^{-2}\mathbf{u}\cdot\mathbf{u}/2\right)$ solves the Fokker-Planck equation, and becomes the invariant measure in the statistical steady state of the system. □

Appendix B. Explicit forms of linear response operators according to Gaussian invariant measure

We focus on the first two leading order moments of the state variables in calculating the linear response operator $\mathcal{R}_A$. The corresponding functionals are then taken as, $A(\mathbf{u}) = \mathbf{u}, \mathbf{u} - \bar{\mathbf{u}}$. Therefore we have the **linear response operators for the mean state**

$$\mathcal{R}_U(t) = \sigma_{\text{eq}}^{-2}\left[a_0\mu\left\langle U'(t)\, U'(0)\right\rangle_{\text{eq}} + \sum_{\mathbf{m}} a_{\mathbf{m}}\left(1 + \frac{\mu}{|\mathbf{m}|^2}\right)\left\langle U'(t)\,\omega'_{\mathbf{m}}(0)\right\rangle_{\text{eq}}\right], \tag{B.1a}$$

$$\mathcal{R}_{\omega_{\mathbf{k}}}(t) = \sigma_{\text{eq}}^{-2}\left[a_0\mu\left\langle \omega'_{\mathbf{k}}(t)\, U'(0)\right\rangle_{\text{eq}} + \sum_{\mathbf{m}} a_{\mathbf{m}}\left(1 + \frac{\mu}{|\mathbf{m}|^2}\right)\left\langle \omega'_{\mathbf{k}}(t)\,\omega'_{\mathbf{m}}(0)\right\rangle_{\text{eq}}\right]. \tag{B.1b}$$

And the **linear response operators for the covariances**

$$\mathcal{R}_{U'^2}(t) = \sigma_{\text{eq}}^{-2}\left[a_0\mu\left\langle U'^2(t)\, U'(0)\right\rangle_{\text{eq}} + \sum_{\mathbf{m}} a_{\mathbf{m}}\left(1 + \frac{\mu}{|\mathbf{m}|^2}\right)\left\langle U'^2(t)\,\omega'_{\mathbf{m}}(0)\right\rangle_{\text{eq}}\right], \tag{B.2a}$$

$$\mathcal{R}_{\omega'^2_{\mathbf{k}}}(t) = \sigma_{\text{eq}}^{-2}\left[a_0\mu\left\langle \omega'^2_{\mathbf{k}}(t)\, U'(0)\right\rangle_{\text{eq}} + \sum_{\mathbf{m}} a_{\mathbf{m}}\left(1 + \frac{\mu}{|\mathbf{m}|^2}\right)\left\langle \omega'^2_{\mathbf{k}}(t)\,\omega'_{\mathbf{m}}(0)\right\rangle_{\text{eq}}\right], \tag{B.2b}$$

$$\mathcal{R}_{U'\omega'_{\mathbf{k}}}(t) = \sigma_{\text{eq}}^{-2}\left[a_0\mu\left\langle \omega'_{\mathbf{k}}(t)\, U'(t)\, U'(0)\right\rangle_{\text{eq}} + \sum_{\mathbf{m}} a_{\mathbf{m}}\left(1 + \frac{\mu}{|\mathbf{m}|^2}\right)\left\langle U'(t)\,\omega'_{\mathbf{k}}(t)\,\omega'_{\mathbf{m}}(0)\right\rangle_{\text{eq}}\right]. \tag{B.2c}$$

These formulations are the direct results by substituting the exact Gaussian distributions (3.8) into the linear response formula (3.4). $\mathbf{a} = \{a_0, a_{\mathbf{k}}\}$ represents the perturbation scales in each mode $\{U, \omega_{\mathbf{k}}\}$.

In the linear response operators for the mean, if we assume the lagged-in-time cross-correlation, $\langle U'(t)\,\omega'_{\mathbf{m}}(0)\rangle$, stays small, the first-order responses can be approximated by the autocorrelation functions for each state variable (but still the exact form of the linear response operator may divert from the autocorrelation function with even large errors due to the contributions from $\langle U'(t)\,\omega'_{\mathbf{m}}(0)\rangle$). And in the linear response operators for second-order statistics, third-order moments for lagged-in-time variables are required. Given hypo-ellipticity, the above dynamical system is provably geometric ergodic [30]. The average under equilibrium measure can be calculated through temporal average along a single trajectory, that is,

$$\left\langle f(t)\, g(0)\right\rangle_{\text{eq}} = \lim_{T\to\infty}\frac{1}{T}\int_0^T f(\tau + t)\, g(\tau)\, d\tau.$$

With the linear response operator $\mathcal{R}_A$ calculated, the leading order FDT prediction can be achieved through (3.3). Especially here we mainly consider the responses to constant perturbation, $\delta\mathbf{F} = \mathbf{a}\delta f \equiv$ const., therefore we only need to consider the time-integrated value R of the linear response operator to get the linear prediction

$$\delta\left\langle A(\mathbf{u})\right\rangle = \int_0^t \mathcal{R}_A(t-s)\,\delta f ds \equiv \delta f R_A, \quad R_A = \int_0^\infty \mathcal{R}_A. \tag{B.3}$$

Using the above formula (B.3) for constant forcing perturbation δf, the leading order responses can be calculated easily and the predictions can be exact if the system is linear. On the other hand, using the integrated form of the linear response operator R_A, many important nonlinear information in the system is neglected (it needs to be emphasized

that the linear response operator, $\mathcal{R}_A$, would include important higher order statistics). This will become a serious problem as the nonlinear interactions between modes become important as we can see in the examples in the main text. This forms the inherent difficulty in prediction using the FDT only. Note that even though in statistical steady state, the invariant measure is Gaussian with U and ω decoupled, the cross-covariance in response becomes non-zero due to the nonlinear structure of the system.

References

[1] M. Lesieur, Turbulence in fluids, Vol. 40, Springer Science & Business Media, 2012.

[2] R. Salmon, Lectures on geophysical fluid dynamics, Oxford University Press, 1998.

[3] J. Pedlosky, Geophysical fluid dynamics, Springer Science & Business Media, 2013.

[4] A. Majda, X. Wang, Nonlinear dynamics and statistical theories for basic geophysical flows, Cambridge University Press, 2006.

[5] C. Franzke, I. Horenko, A. J. Majda, R. Klein, Systematic metastable atmospheric regime identification in an agcm, Journal of the Atmospheric Sciences 66 (7) (2009) 1997–2012.

[6] A. Majda, X. Wang, Linear response theory for statistical ensembles in complex systems with time-periodic forcing, Communications in Mathematical Sciences 8 (1) (2010) 145–172.

[7] A. Gettelman, J. Kay, K. Shell, The evolution of climate sensitivity and climate feedbacks in the community atmosphere model, Journal of Climate 25 (5) (2012) 1453–1469.

[8] J. G. Charney, J. G. DeVore, Multiple flow equilibria in the atmosphere and blocking, Journal of the atmospheric sciences 36 (7) (1979) 1205–1216.

[9] J. E. Hart, Barotropic quasi-geostrophic flow over anisotropic mountains, Journal of the Atmospheric Sciences 36 (9) (1979) 1736–1746.

[10] R. H. Kraichnan, Statistical dynamics of two-dimensional flow, Journal of Fluid Mechanics 67 (01) (1975) 155–175.

[11] A. J. Majda, D. Qi, Improving prediction skill of imperfect turbulent models through statistical response and information theory, Journal of Nonlinear Science 26 (1) (2016) 233–285.

[12] R. H. Kraichnan, D. Montgomery, Two-dimensional turbulence, Reports on Progress in Physics 43 (5) (1980) 547.

[13] G. Holloway, Systematic forcing of large-scale geophysical flows by eddy-topography interaction, Journal of Fluid Mechanics 184 (1987) 463–476.

[14] T. DelSole, Stochastic models of quasigeostrophic turbulence, Surveys in Geophysics 25 (2) (2004) 107–149.

[15] A. J. Majda, B. Gershgorin, Link between statistical equilibrium fidelity and forecasting skill for complex systems with model error, Proceedings of the National Academy of Sciences 108 (31) (2011) 12599–12604.

[16] B. Gershgorin, A. J. Majda, Quantifying uncertainty for climate change and long-range forecasting scenarios with model errors. part i: Gaussian models, Journal of Climate 25 (13) (2012) 4523–4548.

[17] C. Leith, Climate response and fluctuation dissipation, Journal of the Atmospheric Sciences 32 (10) (1975) 2022–2026.

[18] A. Gritsun, G. Branstator, Climate response using a three-dimensional operator based on the fluctuation-dissipation theorem, Journal of the atmospheric sciences 64 (7) (2007) 2558–2575.

[19] A. Gritsun, G. Branstator, A. Majda, Climate response of linear and quadratic functionals using the fluctuation-dissipation theorem, Journal of the Atmospheric Sciences 65 (9) (2008) 2824–2841.

[20] R. V. Abramov, A. J. Majda, A new algorithm for low-frequency climate response, Journal of the Atmospheric Sciences 66 (2) (2009) 286–309.

[21] T. P. Sapsis, A. J. Majda, A statistically accurate modified quasilinear gaussian closure for uncertainty quantification in turbulent dynamical systems, Physica D: Nonlinear Phenomena 252 (2013) 34–45.

[22] T. P. Sapsis, A. J. Majda, Statistically accurate low-order models for uncertainty quantification in turbulent dynamical systems, Proceedings of the National Academy of Sciences 110 (34) (2013) 13705–13710.

[23] A. J. Majda, Statistical energy conservation principle for inhomogeneous turbulent dynamical systems, Proceedings of the National Academy of Sciences 112 (29) (2015) 8937–8941.

[24] A. J. Majda, I. Timofeyev, E. Vanden-Eijnden, Systematic strategies for stochastic mode reduction in climate, Journal of the Atmospheric Sciences 60 (14) (2003) 1705–1722.

[25] J. Harlim, A. Mahdi, A. J. Majda, An ensemble kalman filter for statistical estimation of physics constrained nonlinear regression models, Journal of Computational Physics 257 (2014) 782–812.

[26] E. R. Weeks, Y. Tian, J. Urbach, K. Ide, H. L. Swinney, M. Ghil, Transitions between blocked and zonal flows in a rotating annulus with topography, Science 278 (5343) (1997) 1598–1601.

[27] M. J. Grote, A. J. Majda, C. G. Ragazzo, Dynamic mean flow and small-scale interaction through topographic stress, Journal of Nonlinear Science 9 (1) (1999) 89–130.

[28] G. F. Carnevale, J. S. Frederiksen, Nonlinear stability and statistical mechanics of flow over topography, Journal of Fluid Mechanics 175 (1987) 157–181.

[29] J. S. Frederiksen, M. R. Dix, S. M. Kepert, Systematic energy errors and the tendency toward canonical equilibrium in atmospheric circulation models, Journal of the atmospheric sciences 53 (6) (1996) 887–904.

[30] A. J. Majda, X. T. Tong, Ergodicity of truncated stochastic navier stokes with deterministic forcing and dispersion, accepted by Journal of Nonlinear Science.

[31] A. Majda, An introduction to turbulent dynamical systems in complex systems, 1st Edition, no. 978-3-319-32215-5, Springer International Publishing, 2017.

[32] A. Majda, R. V. Abramov, M. J. Grote, Information theory and stochastics for multiscale nonlinear systems, Vol. 25, American Mathematical Soc., 2005.

[33] S. Kullback, R. A. Leibler, On information and sufficiency, The annals of mathematical statistics 22 (1) (1951) 79–86.
[34] A. J. Majda, C. L. Franzke, A. Fischer, D. T. Crommelin, Distinct metastable atmospheric regimes despite nearly gaussian statistics: A paradigm model, Proceedings of the National Academy of Sciences 103 (22) (2006) 8309–8314.
[35] A. J. Majda, X. T. Tong, Intermittency in turbulent diffusion models with a mean gradient, Nonlinearity 28 (11) (2015) 4171.
[36] D. Qi, A. J. Majda, Predicting fat-tailed intermittent probability distributions in passive scalar turbulence with imperfect models through empirical information theory, Communications in Mathematical Sciences.